Viscoplastic asymptotics and other analytical methods

Neil J. Balmforth

1 Introduction

The goal of these lectures is to outline some of the ideas behind the use of asymptotic analysis and other analytical methods in viscoplastic fluid mechanics (other than variational and bounding techniques, which are covered in lectures by I. Frigaard). General texts on the relevant mathematical methodologies include [9, 25, 47, 43]. Asymptotic analysis surrounds the identification and use of a small parameter to simplify and then solve mathematical problems to build useful approximate solutions. Often, the requirement that a particular parameter is small limits the settings for asymptotic analysis, but the asymptotic developments usually provide key insight by identifying and distilling down the critical physical details and processes. Important phenomenological properties and the scaling with the dimensionless parameters of the problem can then emerge. At the same time, the asymptotic solutions furnish useful limiting test cases for numerical schemes and compact physical predictions.

2 Viscoplastic lubrication theory

2.1 Mathematical formulation

Consider a two-dimensional incompressible viscoplastic fluid slowly flowing down a relatively narrow conduit; flow is driven either by a pressure gradient, the motion of the bounding surfaces, or both. The conduit is described by an arc-length-based curvilinear coordinated system (s, n) following a fixed curve threaded along the length; s is arc-length and n is the normal coordinate. We define $\mathbf{u} = (u, v)$ as the velocity in these coordinates (*i.e.* with respect to the (s, n) axes). Similarly, the deviatoric stress tensor τ_{ij} is also referred to this system. Inertia is neglected.

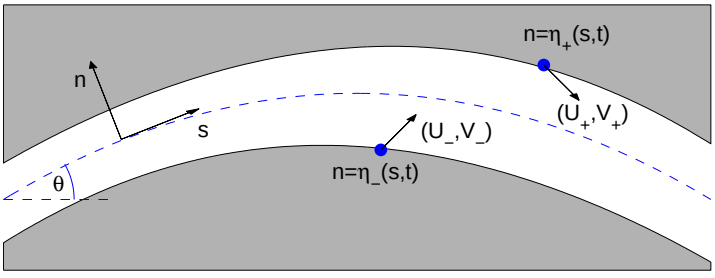

Figure 1: Sketch showing the geometry of a narrow conduit sandwiched between two moving surfaces and filled by a lubricating viscoplastic fluid, together with the arc-length-based coordinates.

Conservation of mass and force balance can be expressed in the form [24]

$$\frac{\partial u}{\partial s} + (1-\kappa n)\frac{\partial v}{\partial n} - \kappa v = 0, \tag{1}$$

$$\frac{\partial \tau_{\rm ss}}{\partial s} + (1-\kappa n)\frac{\partial \tau_{\rm sn}}{\partial n} - 2\kappa\tau_{\rm sn} = \frac{\partial p}{\partial s}, \tag{2}$$

$$\frac{\partial \tau_{\rm sn}}{\partial s} + (1-\kappa n)\frac{\partial \tau_{\rm nn}}{\partial n} + \kappa(\tau_{\rm ss}-\tau_{\rm nn}) = \frac{\partial p}{\partial n}, \tag{3}$$

where κ denotes the curvature.

The strain rate tensor has components,

$$\dot\gamma_{\rm ss} = \frac{2}{1-\kappa n}\left(\frac{\partial u}{\partial s} - \kappa v\right), \quad \dot\gamma_{\rm nn} = 2\frac{\partial v}{\partial n}, \quad \dot\gamma_{\rm sn} = \frac{1}{1-\kappa n}\left(\frac{\partial v}{\partial s} + \kappa u\right) + \frac{\partial u}{\partial n}, \tag{4}$$

which can be fed into the constitutive law:

$$\tau_{ij} = \mu(\dot\gamma)\dot\gamma_{ij} + \tau_Y\frac{\dot\gamma_{ij}}{\dot\gamma}, \quad \text{if } \sqrt{\tau_{\rm ss}^2+\tau_{\rm sn}^2} > \tau_Y, \tag{5}$$

and $\dot\gamma_{ij} = 0$ otherwise, where $\dot\gamma \equiv \sqrt{\dot\gamma_{\rm ss}^2+\dot\gamma_{\rm sn}^2}$.

The upper and lower surfaces are located at $n = \eta_\pm$. Here, the kinematic conditions demand that

$$v = V_\pm = \frac{\partial \eta_\pm}{\partial t} + \frac{U_\pm}{1-\kappa\eta_\pm}\frac{\partial \eta_\pm}{\partial s} \qquad \text{with } u = U_\pm. \tag{6}$$

To identify the principal balance of terms in the limit of a slender gap, one can introduce a characteristic thickness, $\mathcal{H}$, length, $\mathcal{L}$, speed, $\mathcal{U}$, and pressure, $\mathcal{P}$, and then nondimensionalize the variables:

$$\hat s = \frac{s}{\mathcal{L}}, \quad (\hat n, \hat\eta_\pm) = \frac{1}{\mathcal{H}}(n, \eta_\pm), \quad \hat u = \frac{u}{\mathcal{U}}, \quad \hat v = \frac{v\mathcal{L}}{\mathcal{U}\mathcal{H}} \tag{7}$$

and

$$\hat t = \frac{\mathcal{U}t}{\mathcal{L}}, \quad \hat p = \frac{p}{\mathcal{P}}, \quad (\hat\tau, \hat\sigma) = \frac{\mathcal{L}}{\mathcal{H}\mathcal{P}}(\tau_{\rm sn}, \tau_{\rm ss}), \tag{8}$$

The aspect ratio, $\epsilon = \mathcal{H}/\mathcal{L}$, is small when the gap is slender, and this parameter can be used to establish the leading-order relations from the governing equations, and design expansions to proceed to higher order if needed.

The disparate scalings of the two velocity components is guided by the requirement that the gap remains thin and the main balance (to $O(\epsilon)$) in the conservation of mass equation,

$$\frac{\partial \hat u}{\partial \hat s} + \frac{\partial \hat v}{\partial \hat n} = 0. \tag{9}$$

The scaling of the pressure and stress components leads to the main force balances,

$$\frac{\partial \hat p}{\partial \hat s} = \frac{\partial \hat\tau}{\partial \hat n}, \quad \frac{\partial \hat p}{\partial \hat n} = 0. \tag{10}$$

That is, the pressure is largely constant across the slot, but its gradient down that conduit is balanced by the resistance due to the shear stress.

The usual strategy at this stage is to drop the hat decoration that clutters our dimensionless notation and streamline the formulae by exploiting (s, n, t) subscripts to denote partial derivatives (except in the case of the components of the stress and strain-rate tensors, for which we use different font in any case). Following this suit, we write

$$p = p(s,t) \qquad \& \qquad \tau = \tau_-(s,t) + (n - \eta_-)p_s, \tag{11}$$

using the shear stress on the lower surface $\tau_- = \tau(s, \eta_-, t)$. Moreover,

$$\tau_+ - \tau_- = hp_s \tag{12}$$

where $h = \eta_+ - \eta_-$ is the local gap thickness.

The strain rates, scaled by $\mathcal{U}/\mathcal{H}$, become

$$[\dot\gamma_{\rm ss}, \dot\gamma_{\rm sn}] = [2\epsilon u_s, u_n + \epsilon\kappa u] + O(\epsilon^2). \tag{13}$$

At first sight, the disparity in scaling here suggests that the shear rate $\dot\gamma_{\rm sn}$ and therefore the shear stress τ dominate the state of the material to furnish

$$\dot\gamma \sim |\dot\gamma_{\rm sn}| \sim |u_n| \qquad \& \qquad \tau \sim \mu(\dot\gamma)u_n + B\ \mathrm{sgn}(u_n), \tag{14}$$

where $\mu(\dot\gamma)$ is the plastic viscosity scaled by $\mathcal{U}/\mathcal{HP}$ and we (somewhat loosely) refer to the yield-stress parameter $B = \tau_Y/(\epsilon\mathcal{P})$ as a Bingham number.

However, there is another type of solution for the stress state in which $u_n = O(\epsilon)$. In this case, we must have that

$$u \sim u_p(s,t) + \epsilon u_1(s,n,t) + ... \qquad \& \qquad (\dot\gamma_{\rm ss}, \dot\gamma_{\rm sn}) = \epsilon(2u_{ps}, u_{1n} + \kappa u_p) + O(\epsilon^2). \tag{15}$$

The viscous part of the shear stress is then small, but the yield stress contribution demands the stress state is dictated by

$$(\tau, \sigma) = \frac{(\dot\gamma_{\rm ns}, \dot\gamma_{\rm ss})}{\dot\gamma} \qquad \& \qquad \tau^2 + \sigma^2 = B^2. \tag{16}$$

The existence of these two types of stress solutions has in the past caused undue confusion: the so-called "lubrication paradox" [27] surrounds how the use of the first type of solution leads to an apparent inconsistency in the lubrication theory. More specifically, the blind use of this approximation leads to a solution of the problem in which τ appears to fall below B suggesting that the fluid is not yielded and one should then take $u_n = 0$ over a moving "plug" region. But the full solution of the problem (and, in particular, the imposition of the boundary conditions) subsequently indicates that these plugs often cannot be rigid and u still depends on s. *i.e.* the plugs are in extension or compression in the direction of the slot. The resolution of this "paradox" is not that the theory is internally inconsistent, but that one has simply chosen the wrong solution to the stress state, and the second one in (15)(-16) is needed with $u_n = O(\epsilon)$ rather than zero. The plugs are not therefore truly rigid but held close to the yield stress in the fashion of a perfectly plastic material. Walton & Bittleston [46] introduced the terminology "pseudo-plugs" to emphasize this feature of the lubrication problem. The only inconsistency is to implement the first solution in (14) over regions where u_n is not order one.

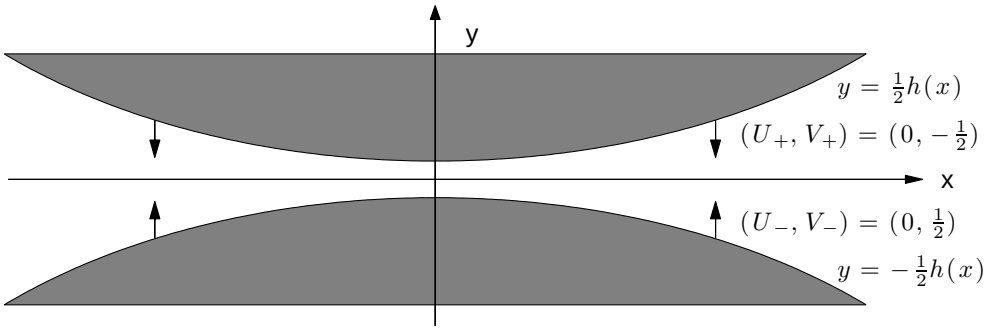

Figure 2: Sketch of a Bingham squeeze flow.

Despite Walton & Bittleston's paper, and several others since (*e.g.* [2, 41, 37]), an unfortunate failing of the literature on viscoplastic flows is to refer to the "lubrication paradox" as though there really were one. This has led to some recent attempts to revise the pseudo-plug solution in an ad hoc and superfluous fashion to try to make that region into a genuinely rigid zone (*e.g.* [21]). Worse, there is even a vein of literature in which it is argued that there are problems with the constitutive law itself and one must regularize to surmount the paradox (*e.g.* [48]). No such deviants are necessary.

The main consequence of all this in the lubrication theory is that one may supplement the fully yielded part of the flow where $u_n = O(1)$ with a region over which u_n is plug-like to complete the asymptotic solution. In most situations u_n is $O(\epsilon)$ and there is a pseudo-plug. In others, one can consistently take $u_n = 0$ and connect the fully yielded region to a true plug. In both cases, this procedure renders no change to the leading-order results and the asymptotic solution is completed in what is effectively the naive manner without worry. We next illustrate all this using a specific model problem, squeeze flow of Bingham fluid between two plates, to make the analysis more transparent and avoid the clutter and opacity of the general formulation. At the same time, this leads us to iron out some finer details of how the fully yielded region fits together (matches) with the pseudo-plug.

2.2 Squeeze flow of Bingham fluid

For the planar problem of squeeze flow of Bingham fluid between two symmetrically approaching surfaces, our curvilinear coordinate system reduces to a Cartesian one: $(s, n) \to (x, y)$. We then have

$$p = p(x, t) \qquad \& \qquad \tau = yp_x, \tag{17}$$

and

$$u(x, \eta_\pm = \pm\tfrac{1}{2}h, t) = 0 \qquad \& \qquad v(x, \eta_\pm = \pm\tfrac{1}{2}h, t) = \mp\tfrac{1}{2}, \tag{18}$$

in view of the symmetry of the problem about $y = 0$, and on fixing the velocity scale $\mathcal{U} = V/\epsilon$ in terms of the closure speed V of the separation of the plates.

If we set $\mathcal{P} = \mu V/\epsilon^2\mathcal{H}$, with $\mathcal{H}$ the initial plate separation, then the constitutive law implies

$$[\tau, \sigma] = (1 + B\dot\gamma^{-1})[u_y, 2\epsilon u_x] + O(\epsilon^2), \tag{19}$$

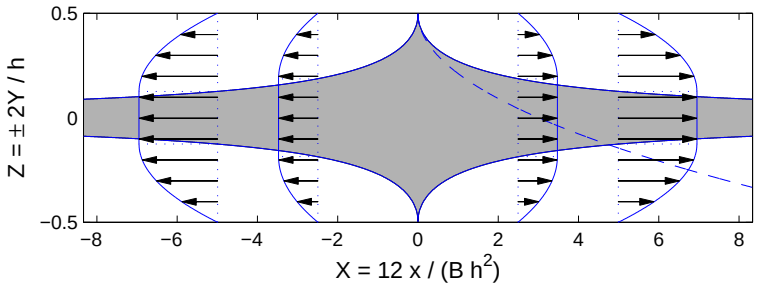

Figure 3: The velocity profile and pseudoplug (shaded) in Bingham squeeze flow. The dashed line shows the approximation, $Y \sim \frac{1}{2}h - \sqrt{x/B}$, for $B \gg 1$.

provided $\tau^2+\sigma^2 < B^2$. Over the fully yield part of the flow, where $\tau = u_y + B\,\mathrm{sgn}(u_y) \gg \sigma$, we now find

$$u_y = (|y| - Y)p_x\,\mathrm{sgn}(y), \qquad Y = \frac{B}{|p_x|}, \tag{20}$$

or

$$u = -\tfrac{1}{2}p_x\left(\tfrac{1}{2}h - |y|\right)\left(\tfrac{1}{2}h - 2Y + |y|\right) \tag{21}$$

(*cf.* figure 3). Moreover, this region occupies $Y < |y| < \frac{1}{2}h$. It is inconsistent to continue this solution into $|y| < Y$ where, instead, $u_y = O(\epsilon)$. In fact, here we must have

$$u = u_p(x,t) + \epsilon u_1(x,y,t), \qquad \text{with} \qquad u_p = -\tfrac{1}{2}p_x\left(\tfrac{1}{2}h - Y\right)^2, \tag{22}$$

in order that the fully yielded solution in (21) be continuous with the pseudo-plug solution $u \sim u_p$.

The $y-$integral of the continuity equation, $u_x+v_y = 0$, in conjunction with the boundary conditions (18), now implies

$$\frac{\partial}{\partial x}\int_{-\frac{1}{2}h}^{\frac{1}{2}h} u\mathrm{d}y = 1. \tag{23}$$

Given the fact that $u(x=0,y,t) = 0$ and

$$\int_{-\frac{1}{2}h}^{\frac{1}{2}h} u\mathrm{d}y \equiv -\int_{-\frac{1}{2}h}^{\frac{1}{2}h} yu_y\mathrm{d}y \equiv -\frac{1}{3}p_x(h+Y)\left(\tfrac{1}{2}h - Y\right)^2, \tag{24}$$

we therefore arrive at an algebraic problem for p_x (recalling that $Y = B/|p_x|$):

$$-\frac{1}{3}p_x[h(x)+Y]\left[\tfrac{1}{2}h(x) - Y\right]^2 = x. \tag{25}$$

From (23), it is clear that the right-hand side corresponds to the net flux down the gap, Q. Hence, equation (25) is the flux-pressure-gradient relation of the lubrication flow: $Q = \frac{1}{3}S(h+Y)(\frac{1}{2}h - Y)^2$, if $S = |p_x|$ denotes the magnitude of the pressure gradient (*cf.* §2.7 below).

Evidently, p_x and therefore Y and u_p depend on position x, highlighting how the flow in $|y| < Y$ is only a pseudo-plug and the curves $|y| = Y(x)$ are fake yield surfaces (in the terminology of Walton & Bittleston). Introducing the variables $Z = Y/h$ and $X = 12x/(Bh^2)$, we may write (25) as a simple cubic for $Z = Z(X)$; the relevant solution for

flat surfaces ($h = constant$) is shown in figure 3, and reproduces one derived by Covey & Stanmore [17].

One application of squeeze flow theory is to compute the lubrication pressure arising between two colliding spheres in a suspension. For the two-dimensional version of this problem, the colliding objects are disks and we may write $h \sim 1 + \frac{1}{2}x^2$ as an approximation of the geometry of the gap when the approach is close. For Newtonian fluid, $Y \to 0$ and we find the classical solution,

$$p_x = -\frac{12x}{h^3}, \qquad \text{or} \qquad p = p_a + \frac{6}{h^2}, \tag{26}$$

where p_a is the ambient fluid pressure. One can then compute the force on the disks, which is to leading order, $\int_{-\infty}^{\infty}(p-p_a)\,\mathrm{d}x$. For a viscoplastic fluid, the situation is rather different: $h \to \frac{1}{2}x^2$ as one moves out of the narrowest part of the gap and the relevant solution of the cubic is

$$Y \to \tfrac{1}{2}h \qquad \& \qquad |p_x| \to \frac{2B}{h}, \qquad \text{or} \qquad p \sim p_a + 2\sqrt{2}B\left[\tfrac{1}{2}\pi - \tan^{-1}\frac{|x|}{\sqrt{2}}\right]. \tag{27}$$

The physical significance of this solution is that the yield stress dominates as one moves out of the gap where the shear rates are in decline. The fake yield surfaces then approach the disk surfaces. Critically, the lubrication pressure, $p - p_a$, is not integrable over the gap, which indicates that the force between the colliding objects is no longer dominated by the lubrication forces over the narrowest parts of the gap. Instead, the force is dictated by the yield stress elsewhere, which complicates the macroscopic description of particle interaction forces in viscoplastic suspensions.

2.3 The pseudo-plug solution and finer matching details

To look at the pseudo-plug more carefully and study how it joins on to the fully yielded flow, we focus on the case of a squeeze flow between flat plates and consider only the first quadrant $(x, y) > 0$ to avoid having to keep track of various sign changes. Given $\sigma^2 + \tau^2 = B^2$ and $\sigma > 0$ because $u_x > 0$, we find that

$$\tau = yp_x \equiv \frac{Bu_{1y}}{\sqrt{4u_{px}^2 + u_{1y}^2}} \qquad \& \qquad \sigma = -p_x\sqrt{Y^2 - y^2} \equiv \frac{2Bu_{px}}{\sqrt{4u_{px}^2 + u_{1y}^2}} \tag{28}$$

over the pseudo-plug. Hence

$$u_{1y} = -\frac{2yu_{px}}{\sqrt{Y^2 - y^2}}. \tag{29}$$

Evidently, $u \to u_p$ from below $y = Y$ and u_{1y} diverges as one approaches that level from the pseudoplug, thus allowing for a larger velocity gradient. These observations do not, however, yet constitute an exercise in matched asymptotics as we appear to be patching two solutions together at a particular point in y.

It turns out that the join is effected over a narrower region surrounding the fake yield surface. To resolve this layer we put

$$y = Y + \delta\zeta \qquad \& \qquad u = u_p + \delta^a U(s, \zeta, t), \tag{30}$$

where $\delta \ll 1$, but its relation with ϵ, and the exponent a both remain to be found. Now, for the fully yielded region we have $\dot{\gamma} \sim |u_y|$, whereas we know that $\dot{\gamma} \sim \epsilon\sqrt{4u_{px}^2 + u_{1y}^2}$ over the pseudo-plug. To connect these two limits, we therefore introduce the approximation $\dot{\gamma} \approx \sqrt{\delta^{2a-2}U_\zeta^2 + 4\epsilon u_{px}^2}$ into the constitutive law:

$$\tau \equiv -B + \delta\zeta p_x \approx \delta^{a-1}U_\zeta + \frac{B\delta^{a-1}U_\zeta}{\sqrt{\delta^{2a-2}U_\zeta^2 + \epsilon^2 u_{px}^2}}. \tag{31}$$

Given $U_\zeta < 0$, the main balance of terms in this relation is just $-B \approx -B$; demanding that the next-order corrections all have the same size implies $a = 2$ and $\delta = \epsilon^{2/3}$. Thence, we arrive at

$$U_\zeta^3 - \zeta p_x U_\zeta^2 + 2Bu_{px}^2 \approx 0. \tag{32}$$

This cubic has a real solution that converges to the limit $U_\zeta \sim \zeta p_x$ for $\zeta \to \infty$, and to the limit $U_\zeta \sim -u_{px}\sqrt{2B/\zeta p_x}$ for $\zeta \to -\infty$; *i.e.* the limits of the fully yielded and pseudo-plug solutions for $y \to Y$. In other words, the pseudo-plug can be matched to the fully yielded flow over a thin layer of thickness $\epsilon^{2/3}$.[1]

2.4 Strategy for more general solutions

Returning to more general situations, we express the shear rate u_n in terms of the shear stress using the inverse of the constitutive law,

$$u_n = \Gamma(\tau) \tag{33}$$

(see figure 4). Unlike the original law, which is multi-valued for $\tau < \tau_Y$, this inverse is unambiguous with $u_n = 0$ for that range of stress (although the interpretation is not that the fluid is rigid, but that it may be a pseudo-plug). We may integrate this equation over the gap and change the integration variable from

$$n \equiv \frac{\tau - \tau_-}{p_s} + \eta_- \equiv h\frac{\tau - \tau_-}{\tau_+ - \tau_-} + \eta_- \tag{34}$$

to τ:

$$U_+ - U_- = \int_{\eta_-}^{\eta_+} u_n \mathrm{d}n = h\frac{I_0(\tau_+) - I_0(\tau_-)}{\tau_+ - \tau_-}, \tag{35}$$

where, as illustrated in figure 4,

$$I_j(\tau) = \int^\tau z^j \Gamma(z)\mathrm{d}z. \tag{36}$$

We may also integrate our continuity relation, $u_s + v_n = 0$, in n and use the kinetic conditions on the bounding surfaces to arrive at

$$h_t + \frac{\partial}{\partial s}\int_{\eta_-}^{\eta_+} u \, \mathrm{d}n = 0. \tag{37}$$

[1]The corresponding analysis presented in Balmforth & Craster [2] contains erroneous powers; Putz, Frigaard & Martinez [37] previously provide corrected formulae.

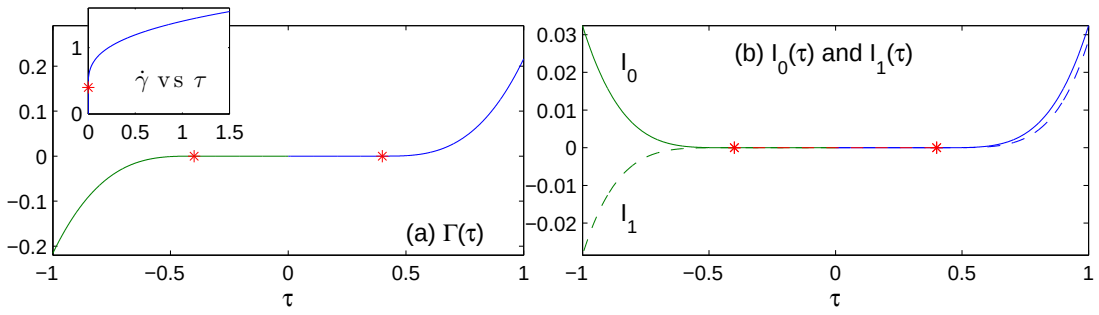

Figure 4: Illustration of the inverse of the Herschel-Bulkley law ($\tau = K\dot\gamma^n + \tau_Y$, where K is the consistency and n the power-law index) and the $I_j(\tau)$ functions it generates, for power-law index $n = \frac{1}{3}$.

Hence,

$$Q(t) = \int_0^s h_t(s',t)\mathrm{d}s' + U_+\eta_+ - U_-\eta_- - h^2\frac{I_1(\tau_+) - I_1(\tau_-)}{(\tau_+ - \tau_-)^2} + h^2\tau_-\frac{I_0(\tau_+) - I_0(\tau_-)}{\tau_+ - \tau_-}, \quad (38)$$

where Q is an integration constant. Equations (35) and (38) constitute an algebraic problem to solve for the surface shear stresses $\tau_\pm(s,t)$ given the constitutive functions $I_j(\tau)$, the instantaneous geometry of the gap and the motion of the bounding surfaces. A further relation is needed to determine $Q(t)$. In some problems (like in the squeeze flow problem) a spatial symmetry can be used to fix this quantity; in others, the pressure drop Δp across the slot is known and so we have an additional relation,

$$\Delta p = \int p_s \mathrm{d}s = \int (\tau_+ - \tau_-)\frac{\mathrm{d}s}{h}. \quad (39)$$

Note that the problem here is parameterized in terms of the surface shear stresses $\tau_\pm$, which hides and avoids an otherwise complicating feature of the problem: at no stage is there a need to recognise the detailed flow configuration. Instead, one constructs after $\tau_\pm$ are determined. The issue that one would otherwise face is that with general motions allowed for the boundaries and an initially unkown pressure gradient along the gap, there are many possibilities for the form of the flow within the conduit: there may be moving pseudo-plugs, genuinely rigid zones attached to the walls or neither. If one were to work with the velocity field directly, the solution strategy would necessarily require a first effort to find the relevant flow configuration. However, by working with $\tau_\pm$, and because the shear stress itself varies only linearly across the gap, this task is avoided. After determining the surface stresses, one can identify the flow configuration based on how they compare to B (see figure 5):

- A: Fully yielded zone; $|\tau_-|, |\tau_+| > B$ and $\mathrm{sgn}(\tau_-) = \mathrm{sgn}(\tau_+)$.
- B: Lower plug; $|\tau_-| < B$.
- C: Central pseudo-plug; $|\tau_-|, |\tau_+| > B$ and $\mathrm{sgn}(\tau_-) = -\mathrm{sgn}(\tau_+)$.
- D: Upper plug; $|\tau_+| < B$.

The preceding formulation is a slight generalization of that presented by Hewitt & Balmforth [24]. They provide a number of examples for illustration, including viscoplastic

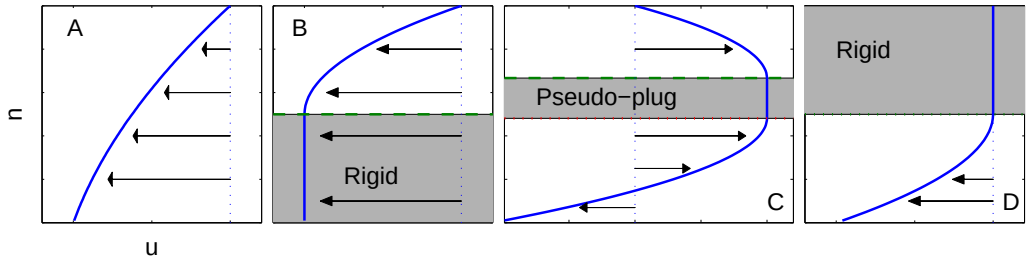

Figure 5: Examples of the four possible flow configurations.

journal and slider bearings [35], and indicate further how the construction can be made computationally efficient and be used to dynamically evolve the gap or film (if one the surfaces is free). Figure 6 shows one of their journal bearing solutions in which the two cylinders of the bearing have prescribed rotation rates and translation speeds with respect to one another. Here, the arc-length coordinate here simply corresponds to angle, and the solution contains all of the flow configurations indicated above over different angular locations of the gap. Also shown is the pressure distribution (here $\Delta p = 0$ in view of the periodic geometry) and the plug speed $u_p(s)$, which varies in the pseudo-plugs, but is constant in configurations B and D when the plug is truly rigid and attached to one of the cylinders. Figure 7 shows a slider bearing solution (with no net pressure drop underneath, $\Delta p = 0$). Again, the full flow solution contains all four possible configurations.

2.5 Plastic limit

Returning to the Bingham squeeze flow problem, an interesting limit arises for $B \gg 1$. For such a parameter setting, the fake yield surfaces, $y = \pm Y$, must approach the bounding plates, $y = \pm\frac{1}{2}h$ (the solution of the cubic in (25) lies near $X = 0$ in figure 3). Thus $p_x \to -2B/h$ (or $p \to -2Bx/h$) and we arrive at

$$Y \sim \tfrac{1}{2}h - \sqrt{B^{-1}x}. \tag{40}$$

The fully yielded flow therefore becomes restricted to boundary layers of thickness $B^{-1/2}$. The pseudo-plug, on the other hand, has the stress solution,

$$(\tau, \sigma) \sim B\left(-\frac{2y}{h}, \sqrt{1 - \frac{4y^2}{h^2}}\right), \tag{41}$$

and plug speed $u_p \sim x/h$.

It is informative to compare the solution (41) with a classical solution of Prandtl in ideal plasticity theory [36]. This solution pertains to the squeeze flow of an ideal plastic material without any immediate assumption regarding the slenderness of the configuration. Indeed, one can check that (41), together with the pressure solution

$$p = -\frac{2Bx}{h} - B\sqrt{1 - \frac{4y^2}{h^2}}, \tag{42}$$

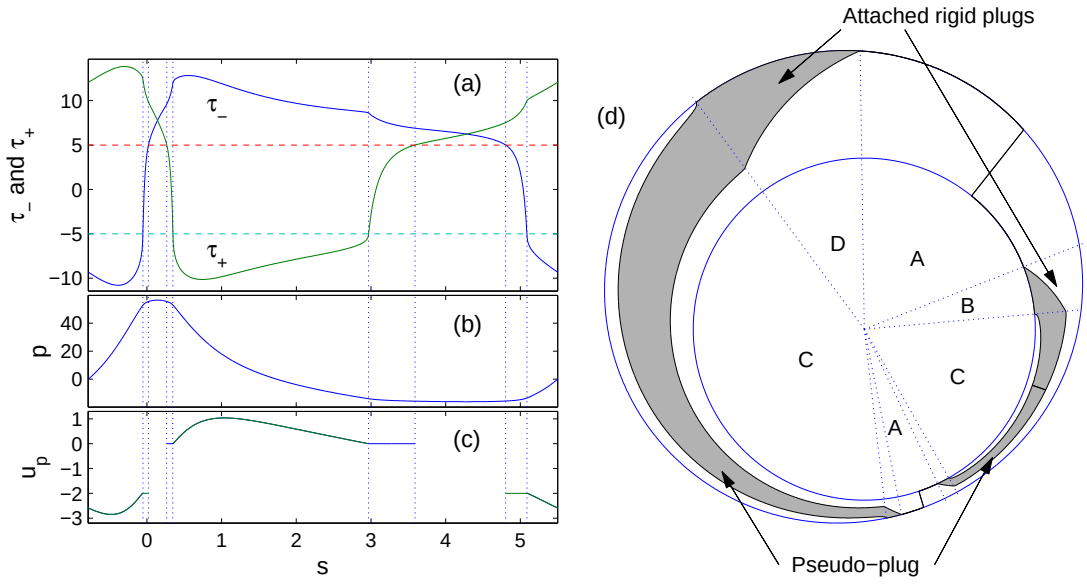

Figure 6: A viscoplastic journal bearing solution, showing (a) $\tau_\pm(s)$, (b) $p(s)$, (c) $u_p(s)$ and (d) the fully yielded regions, true plugs and pseudo-plugs. The dotted lines show the borders of the regions with different flow configurations (as indicated in (d)). In (a), the dashed lines show $\pm B$. The origin of s (which corresponds to angle) is the location of the minimum gap. The outer cylinder (of radius 1.1) is fixed in place whilst the inner cylinder (of radius 0.8) rotates with angular speed 2 and its centre moves in the direction of the line of centres so as to close the minimum gap at speed 1. The fluid has a Bingham number of $B = 5$ and a power-law index of $n = \frac{1}{2}$.

satisfies the full force-balance equations,

$$\frac{\partial}{\partial x}(\sigma - p) + \frac{\partial \tau}{\partial y} = 0 \qquad \& \qquad \frac{\partial \tau}{\partial x} - \frac{\partial}{\partial y}(\sigma + p) = 0, \tag{43}$$

along with the yield condition $\sigma^2 + \tau^2 = B^2$. In other words, our pseudo-plug solution is nothing more than the shallow limit of Prandtl's solution. Importantly, the presence of the fully yielded boundary layer adjacent to the plates is equivalent to Prandlt's assumption that those surfaces are "fully rough." That is, u must vanish on the plates whatever the stress exerted there, implying $u_x = 0$ and therefore $\sigma = 0$.

2.6 Sliplines

In ideal plasticity, an elegant way of solving (43) is using the method of characteristics [36]. This method constructs two families of special curves along which certain quantities are conserved, all of which can be recognized by defining

$$(\sigma, \tau) = B(-\sin 2\vartheta, \cos 2\vartheta), \tag{44}$$

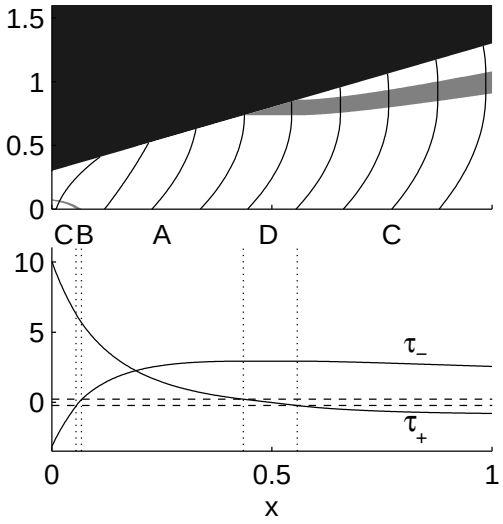

Figure 7: A viscoplastic slider bearing solution, showing on top the geometry, true and pseudo plugs (shaded) and sample horizontal velocity profiles (solid lines), and on the bottom the surface shear stresses $\tau_\pm(x)$. The inclined slider (of length 1) moves to the right with speed 1. The dotted lines show the borders of the regions with different flow configurations (as indicated), and the dashed lines show $\pm B = 0.2$ (with power-law index $n = 1$). There are small C and B regions underneath the slider near the narrowest part of the gap.

and then rewriting (43) in the two forms,

$$\left(\cos\vartheta\frac{\partial}{\partial x}+\sin\vartheta\frac{\partial}{\partial y}\right)(p+2B\vartheta)=\left(\sin\vartheta\frac{\partial}{\partial x}-\cos\vartheta\frac{\partial}{\partial y}\right)(p-2B\vartheta)=0. \qquad (45)$$

In plasticity theory, the two families of characteristic curves are called sliplines and have parametric equations,

$$\frac{\mathrm{d}y}{\mathrm{d}x}=\tan\vartheta \qquad \& \qquad \frac{\mathrm{d}y}{\mathrm{d}x}=-\cot\vartheta. \qquad (46)$$

Evidently the two sets of sliplines are orthogonal to one another, and along these curves the (Riemann) invariants are $p \pm 2B\vartheta$ (respectively). The sliplines for Prandtl's squeeze flow solution, given in $x > 0$ by

$$\frac{x-x_0}{h}=\pm\tan^{-1}\sqrt{\frac{\frac{1}{2}h+y}{\frac{1}{2}h-y}}-\sqrt{1-\frac{4y^2}{h^2}}, \qquad (47)$$

where $x = x_0$ is the starting point of the curve on the bottom plate, are illustrated in figure 8. (The slipline pattern has reflection symmetry about both coordinate axes.)

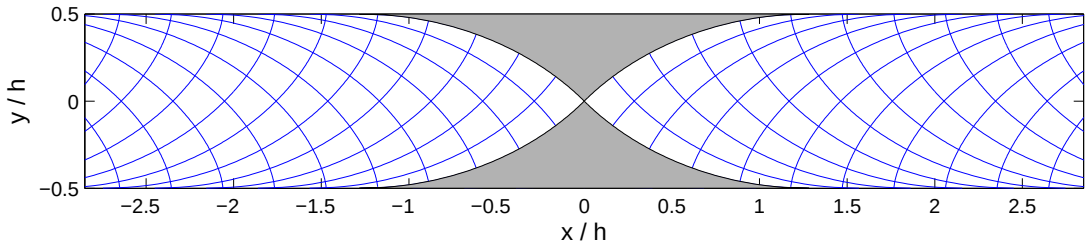

Figure 8: Prandtl's slipline solution with the central plugs shaded.

Although it is not a slender approximation, Prandtl's solution requires correction at the edges and core of the squeeze flow [41, 42]: at the edges, the flow must be terminated

somehow, perhaps by allowing the fluid to extrude into free space beyond the ends of the plate. At the centre, the slipline pattern must be adjusted to allow for the symmetry condition along $x = 0$. One way to do this is to assume that the sliplines that intersect the origin are yield surfaces and enclose a plug, as indicated in figure 8. Such a construction is allowed because further theory of the slipline field establishes that any of the sliplines can play the role of a yield surface provided the resulting stress field is consistent.

In more general geometries, the construction of the slipline network is more challenging. Practically, the most straghtforward situation is when p and ϑ are both known along a given curve. The sliplines can then be constructed by integrating (46) out from the known curve into the region of plastic deformation, exploiting the known invariants $p \pm 2B\vartheta$ and perhaps a simple finite-difference approximation [36]. Unfortunately, only in a limited number of problems does one have the necessary known curve. More often, one must a boundary-value type problem because one only has incomplete information on more than one curve. Worse, problems in which boundary conditions on the velocity are required demand a simultaneous calculation of the velocity field. Despite this, slipline theory has proved useful in some specific plasticity problems that can be viewed as the plastic limits of viscoplastic flow problems [31, 38, 14]) Alternatively, a useful test of the fidelity of a numerical scheme in the plastic limit can be provided by examining the slipline field predicted by a computed solution.

Note that the length of the adopted plugs in figure 8 is of the same order as the slot thickness and are therefore inaccessible in the lubrication theory even if the slot is narrow. Indeed, as discussed in [46, 37], one expects that true plugs could be hidden within the pseudo-plugs of slender flows around points of symmetry or stagnation; their detection and characterization requires a less controlled approximation strategy in view of their lack of scale separation. When the geometry of the conduit itself is more complicated, plugs can also clog wells and corners if their lengths are too short [39].

2.7 Extension to three dimensions

The lubrication analysis can be readily extended to three dimensions. We summarize the generalization for Herschel-Bulkley fluid flowing down a largely planar slot that is symmetrical about its midplane. The flow is pressure-driven and the walls are fixed in time. We align the midplane with the $(x, z)-$coordinate plane ($y = 0$; see figure 9). The dominant balance of forces is then

$$\frac{\partial p}{\partial x} = \frac{\partial \tau_{xy}}{\partial y}, \quad \frac{\partial p}{\partial y} = 0, \quad \frac{\partial p}{\partial z} = \frac{\partial \tau_{zy}}{\partial y}, \tag{48}$$

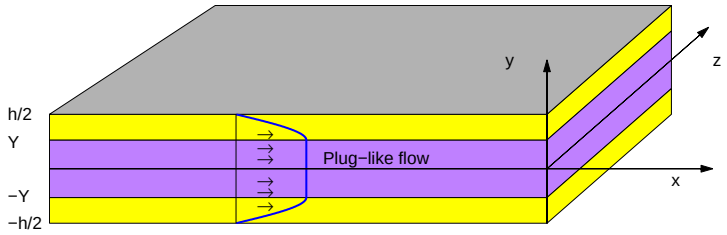

Figure 9: Sketch of the geometry for a viscoplastic fluid in a Hele-Shaw cell.

leading to

$$p = p(x,z), \quad (\tau_{\rm xy}, \tau_{\rm zy}) = z\,(p_x, p_z)\,. \tag{49}$$

The shear rates (u_y, w_y) across the slot again dominate the strain-rate tensor. Hence, the consitutive law, suitably non-dimensionalized using the characteristic viscosity $\mu_* = K(\mathcal{U}/\mathcal{H})^{n-1}$ where K is the consistency and n is the power-law index, indicates that

$$\begin{pmatrix} \tau_{\rm xy} \\ \tau_{\rm zy} \end{pmatrix} \approx \left(\dot\gamma^{n-1} + \frac{B}{\dot\gamma}\right) \begin{pmatrix} u_y \\ w_y \end{pmatrix} \quad \text{if} \quad \tau \approx \sqrt{\tau_{\rm xy}^2 + \tau_{\rm zy}^2} > B, \tag{50}$$

where

$$\dot\gamma \approx \sqrt{u_y^2 + w_y^2}. \tag{51}$$

The (u, w) velocity field now follows (see figure 9):

$$\begin{pmatrix} u \\ w \end{pmatrix} = -\frac{n}{n+1} S^{(1-n)/n} \left[\max(\tfrac{1}{2}h - Y, 0)^{(n+1)/n} - \max\left(|y| - Y, 0\right)^{(n+1)/n}\right] \begin{pmatrix} p_x \\ p_z \end{pmatrix}, \tag{52}$$

where the "yield surface" and pressure gradient are

$$Y = \frac{B}{S} \qquad \& \qquad S = \sqrt{p_x^2 + p_z^2}. \tag{53}$$

Note that, in the squeeze flow problem of §2.2, flow was immediately forced by the motion of the walls. For the current, pressure-driven flow, the pressure gradient may not always be sufficient to drive fluid down the slot, in which case the conduit must clog up and a true plug bridge the gap. Mathematically, this translates to Y exceeding $\frac{1}{2}h$ in the formulae above; the switch, $\max(\frac{1}{2}h - Y, 0)$, takes care of the implied (genuine) yield condition.

We now define a streamfunction based on the flux down the slot:

$$\begin{pmatrix} -\psi_z \\ \psi_x \end{pmatrix} = \int_{-\frac{1}{2}h}^{\frac{1}{2}h} \begin{pmatrix} u \\ w \end{pmatrix} \mathrm{d}y. \tag{54}$$

After a little algebra one then finds

$$\begin{pmatrix} \psi_z \\ -\psi_x \end{pmatrix} = \frac{Q}{S} \begin{pmatrix} p_x \\ p_z \end{pmatrix}, \tag{55}$$

involving the flux-pressure-gradient relation,

$$Q \equiv \sqrt{\psi_x^2 + \psi_z^2} = \frac{2n}{(n+1)(2n+1)} \left[\max\left(\tfrac{1}{2}h - Y\right), 0)\right]^{1+1/n} [\tfrac{1}{2}(n+1)h + nY] S^{1/n}, \tag{56}$$

which is plotted in figure 10 (for $n = 1$). Finally, $p_{zx} = p_{xz}$ implies

$$(Q^{-1} S \psi_x)_x + (Q^{-1} S \psi_z)_z = 0, \tag{57}$$

a nonlinear elliptic equation that is similar to models proposed for viscoplastic displacement flows and nonlinear filtration (*e.g.* [11, 33]).

For a Newtonian fluid, $Q \to (h^3/12)S$, (57) reduces to Laplace's equation and (56) is equivalent to Darcy's law, thus connecting flow in a Hele-Shaw cell with that through

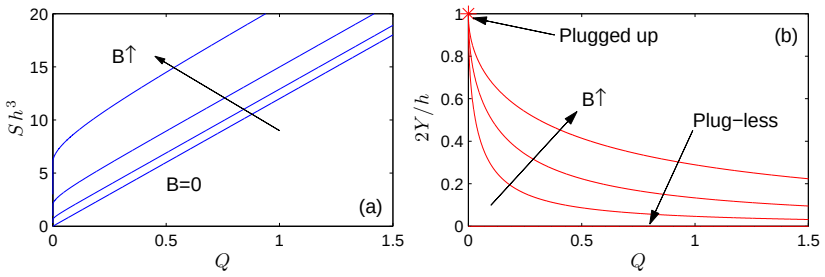

Figure 10: (a) Flux-pressure-gradient relation for Bingham flow down a Hele-Shalw cell. (b) shows the corresponding fake yield surface. ($n = 1$)

a porous medium. By analogy with this connection, and with a more general relation between Q and S than in (56), the nonlinear elliptic problem in (57) has been posed as a model for viscoplastic flow through a porous medium (*e.g.* [19]). Recent computations and experiments have even attempted to calibrate the $Q - S$ relation for particular idealized porous media [15, 44, 12], following on from earlier Russian literature focussed on oil recovery problems (*e.g.* [10]). Importantly, as for the original viscoplastic constitutive law, the $Q - S$ relation features a threshold for flow to begin (figure 10), corresponding to the yield condition encoded in the switch, $\max(\frac{1}{2}h - Y, 0)$.

The connection between Newtonian flow through a slot and in a porous medium originally motivated Henry Selby Hele-Shaw to visualize potential flow around obstacles. Along this vein, some numerical solutions to the model in (56)-(57) are shown in figure 11 for viscoplastic flow around a disk and an ellipse (obtained using an Augmented Lagrangian algorithm, see lectures by A. Wachs). These solutions contain genuine plug regions fore and aft of the obstacles, where Y reaches $\frac{1}{2}h$, $Q \to 0$ and flow grinds to a halt.

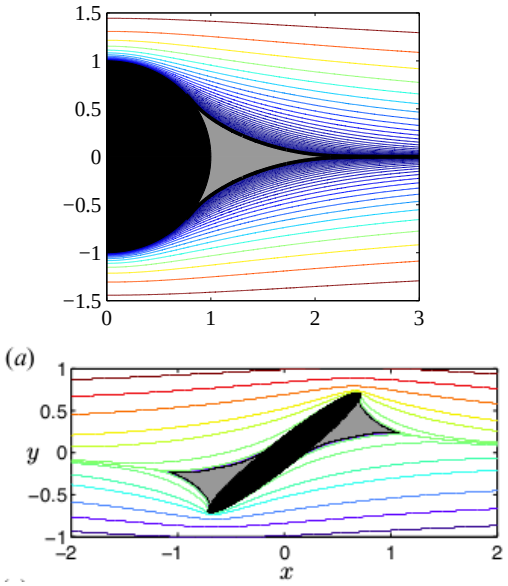

Figure 11: Viscoplastic flow around a disk and an ellipse in a uniform Hele-Shaw cell with $B = 32$ and 20, respectively. Shown are a selection of streamlines. Lengths and velocities are scaled such that the mean flux in the $x-$direction is 2 well upstream or downstream of the obstacles, which have unit radius or semi-major axis, and the half-thickness of the cell is unity. Obstacles are shaded black; plugs are grey.

A clever way to deal with (57) (and some other viscoplastic flow problems [19]) is to use the Hodograph transformation, which can be applied when the slot is uniform (h is

constant): this technique introduces the polar coordinate representations,

$$\begin{pmatrix} p_x \\ p_z \end{pmatrix} = S \begin{pmatrix} \cos\Theta \\ \sin\Theta \end{pmatrix} \qquad \text{and} \qquad \begin{pmatrix} \psi_x \\ \psi_z \end{pmatrix} = Q \begin{pmatrix} \sin\Theta \\ -\cos\Theta \end{pmatrix}, \tag{58}$$

and then makes the transformation, $(x, y) \to (Q, \Theta)$. The result is a linear elliptic problem for the streamfunction [19]:

$$\frac{Q^2}{S}\left(\frac{S^2}{QS'}\psi_Q\right)_Q + \psi_{\Theta\Theta} = 0, \tag{59}$$

along with

$$p_\Theta = -\frac{S^2}{QS'}\psi_Q, \qquad p_Q = \frac{S}{Q^2}\psi_\Theta, , \tag{60}$$

where $S' = \mathrm{d}S/\mathrm{d}Q$. Although the original elliptic equation is thereby linearized, the practical use of the Hodograph transformation is limited because one can only impose the boundary conditions after mapping the problem back to real space, which can prohibitively complicate those conditions.

Despite this, one can manufacture exact solutions for some special problems. For example, an interesting separable solution of (59) is given by $\psi = a(Q)\sin 2\Theta$ (*cf.* [1]), where

$$\frac{Q^2}{S}\left(\frac{S^2}{QS'}a_Q\right)_Q - 4a = 0, \tag{61}$$

subject to the limits $a \propto Q^\alpha$ as $Q \to \infty$ and $a \propto Q^{(2n+1)/(n+1)}$ as $Q \to 0$ (which correspond to matching the solution to a far-field flow of power-law fluid and demanding that the pressure remains finite when flow halts), where

$$\alpha = \tfrac{1}{2}\sqrt{(n-1)^2 + 16n} - \tfrac{1}{2}(n-1). \tag{62}$$

The corresponding streamline pattern of the solution can be found by integrating

$$\left(\frac{\mathrm{d}x}{\mathrm{d}\Theta}, \frac{\mathrm{d}y}{\mathrm{d}\Theta}\right) = S^{-1}\frac{\mathrm{d}p}{\mathrm{d}\Theta}(\cos\Theta, \sin\Theta) \tag{63}$$

along curves of constant ψ, as illustrated in figure 12 for $n = 1$. Evidently, this solution corresponds to a stagnation-point flow with an embedded plug. The yield surfaces bordering this region can be constructed analytically (exploiting the fact that this curve is the limiting streamline for $Q \to 0$, along which $p \propto \cos 2\Theta$); in the first quadrant,

$$(x, y) = c(n)B^{(\alpha-1)/n}(\cos 3\Theta + 3\cos\Theta, 3\sin\Theta - \sin 3\Theta), \tag{64}$$

where $c(n)$ is an $n-$dependent constant that is determined from integrating the ODE in (61). Further details, as well as a discussion of other types of solutions can be found in [1, 19, 10, 23].

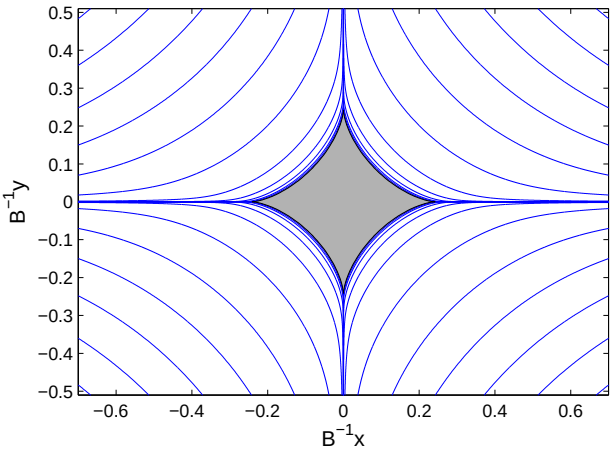

Figure 12: Stagnation-point flow in a Hele-Shaw cell filled with Bingham fluid, matching to $\psi = 2xy$ in the far field.

3 Viscoplastic boundary layers

The fully yield boundary layer arising in lubrication theory for $B \gg 1$ is an example of a viscoplastic boundary layer, in the sense that over this relatively thin region both viscous stresses and the yield stress complete the balance of forces. However, this is not the only situation in which viscoplastic boundary layers can arise. Indeed, Oldroyd [32] in a classical paper suggested how such layers might arise in a variety of contexts and presented an analysis of the possible boundary-layer structure for Bingham fluid. A drawback of Oldroyd's theory is that it requires the solution of a rather challenging-looking PDE, and likely as a consequence, there have no attempts since to solve the problem in general settings. Oldroyd did, however, show that the equation had solutions with similarity form. Nevertheless, the relevance of these solutions has never been confirmed in any particular flow configuration. Moreover, the boundary layer structure (an in particular its scaling with Bingham number) appears to be different than in Oldroyd's theory in a number of other contexts [45, 13].

3.1 Oldroyd's viscoplastic shear layer

Oldroyd's shear layer is the border between two plug flows which becomes thin in the limit that the Bingham number, $B = \mathcal{H}\tau_Y/(\mu\mathcal{U})$, is large, where $\mathcal{H}$ is a characteristic thickness of the layer and $\mathcal{U}$ is the velocity jump across it. For a straight boundary layer orientated along the horizontal line $y = y_0$ and with a characteristic aspect ratio of thickness to length of $\varepsilon \ll 1$, we resolve the boundary layer with a stretched coordinate and rescale for $B = \varepsilon^{-3} \gg 1$:

$$y = y_0 + \varepsilon\zeta, \quad u = u_m + U(x,\zeta), \quad v = \varepsilon V(x,\zeta), \tag{65}$$

where u_m is the mean horizontal velocity of the boundary layer, and

$$p = \frac{P(x,\zeta)}{\varepsilon^2}, \quad \tau = -\frac{1}{\varepsilon^3} + \frac{\check{\tau}(x,\zeta)}{\varepsilon}, \quad \sigma = \frac{\check{\sigma}(x,\zeta)}{\varepsilon^2}, \tag{66}$$

assuming $u_y < 0$, so that the leading-order shear stress is $\tau = -B$. These rescalings are designed so that, although τ dominates the stress state, the extensional stresses and pressure

gradient still enter the force balance along with that dominant component. The consequence of this design is that the thickness of the boundary layer has the scaling $\varepsilon = B^{-1/3}$.

The rescaled conservation equations are, to leading order,

$$U_x + V_\zeta = 0, \qquad P_x = \frac{\partial \check{\tau}}{\partial \zeta} + \frac{\partial \check{\sigma}}{\partial x} \qquad \& \qquad P_\zeta = -\frac{\partial \check{\sigma}}{\partial \zeta} + O(\varepsilon^2). \tag{67}$$

The expansion of the constitutive law for yielded fluid gives

$$\check{\tau} = U_\zeta + \frac{2U_x^2}{U_\zeta^2} \qquad \& \qquad \check{\sigma} = -\frac{2U_x}{U_\zeta} \tag{68}$$

Eliminating the pressure furnishes Oldroyd's boundary-layer equation,

$$\left[U_\zeta + \frac{2U_x^2}{U_\zeta^2}\right]_{\zeta\zeta} - 4\left(\frac{U_x}{U_\zeta}\right)_{x\zeta} = 0. \tag{69}$$

3.2 Self-similar solutions

As indicated by Oldroyd, the boundary-layer equations have a solution with the self-similar form,

$$U = f(\chi) \qquad \& \qquad \chi = \frac{\zeta}{Y(x)}. \tag{70}$$

Assuming anti-symmetry about the centreline of the boundary-layer, and plugging (70) into (69), we find

$$f_{\chi\chi} = \lambda\chi \qquad \& \qquad Y_{xx} = -\frac{\lambda}{4Y^2}, \tag{71}$$

where λ is a separation constant. Imposing $f = \mp\frac{1}{2}$ and $f_\chi = 0$ at $\chi = \pm 1$ now gives

$$f = \tfrac{1}{4}\chi(\chi^2 - 3) \qquad \& \qquad \lambda = \frac{3}{2}. \tag{72}$$

One then has to solve (71a) for Y. There are solutions with $Y = Y_e$ and $Y_x = 0$ at the right-hand end of the boundary layer (giving $U_x = 0$) with

$$Y_e^{3/2}\left[\tan^{-1}\sqrt{\frac{s}{1-s}} - \sqrt{s(1-s)}\right]_{s=Y_0/Y_e}^{Y/Y_e} = \frac{\sqrt{3}}{2}(x - x_0), \tag{73}$$

where $(x, Y) = (x_0, Y_0)$ denotes the start of the boundary layer. For $Y_e \to \infty$, we recover Oldroyd's power-law solution, $Y \propto x^{2/3}$.[2]

[2]The determination of solutions of similarity form is a mathematical subject of itself. One option for the task is to introduce the rescalings, $(\hat{x}, \hat{\zeta}) = (kx, \ell\zeta)$, and then to establish what combinations (if any) of the parameters k and ℓ lead to the same equation as (69). One finds this to be so if $k^2 = \ell^3$. The combination $\chi = x/\zeta^{3/2} = \hat{x}/\hat{\zeta}^{3/2}$ is therefore invariant under the transformation and implies the existence of a self-similar solution with $U = U(\eta)$.

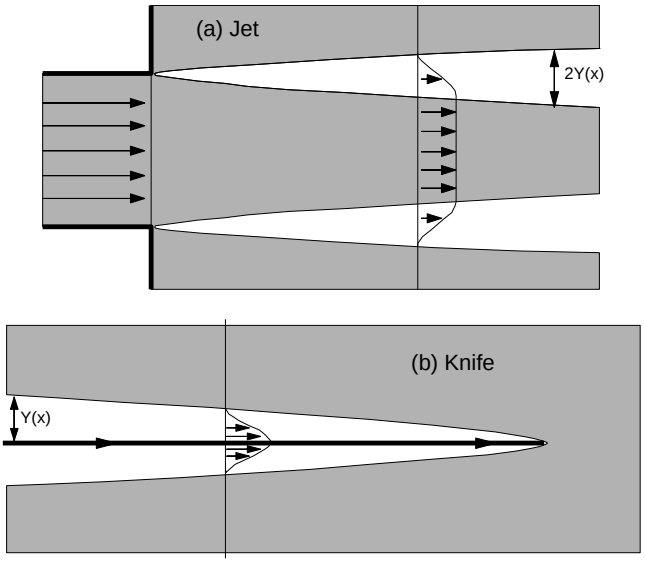

Figure 13: Oldroyd's two canonical boundary layer problems: (a) A jet or finger of unyielded viscoplastic fluid is pushed out of a vent in a wall into a semi-infinite region filled with stagnant fluid; two thin shear layers buffer the plugged core of the jet from the rigid ambient. (b) The flow around a knife or plate pushed through an infinite viscoplastic fluid; a viscoplastic boundary layer coats the moving object.

3.3 Sample flow solutions with boundary layers

Oldroyd suggested two canonical problems in which viscoplastic boundary layers might appear. The first consists of a finger or jet of Bingham fluid pushed out of a vent in a wall into semi-infinite region filled with stagnant fluid (see figure 13(a)). Oldroyd proposed that the borders between the finger and ambient would yield to form two thin viscoplastic shear layers with structure given by (72)-(73). Figure 14 shows a numerical solution of this problem, but set in a finite domain (with symmetry conditions imposed to the right and on the top and bottom) and computed using an augmented Lagrangian scheme. As predicted by Oldroyd, the sides of the finger form widening shear layer whose thickness scales with $B^{-1/3}$. The velocity profile and shape of the shear layer both agree with the self-similar solution.

Note that if one considers a narrower jet entering the same domain the solution is qualitatively different: the fluid yields almost immediately as it leaves the vent to form a wide plastically deforming region (figure 15); the plastic zones begin at the edges of the vent and merge together, leaving a small triangular tip to the incoming rigid jet. The plastic zone subsequently splits apart again further down the extrusion at a yield surface that eventually closes off the plastic region. Two horizontal viscoplastic boundary layers then remain that divide the surrounding rigid ambient from a moving plugged jet, and whose structure is again predicted by Oldroyd's self-similar solution. Thus, the extrusion adjusts to provide a minimum jet thickness if the vent is too narrow, and Oldroyd's expected flow configuration is recovered downstream.

As illustrated in figure 15(c,d), the solution over the plastic region is described by a slipline field that begins with two expansion fans centred at the vent's edges and meets the symmetry line along the axis of the jet ($y = 0$) at $\pm 45°$ (a consequence of $\tau = 0$ there). The sliplines that border the triangular tip of the rigid jet form straight lines inclined at 45°. In turn, this implies that all the other sliplines of the same family in the fan form (straight) radial spokes of equal length and that the other family forms a set of concentric circular

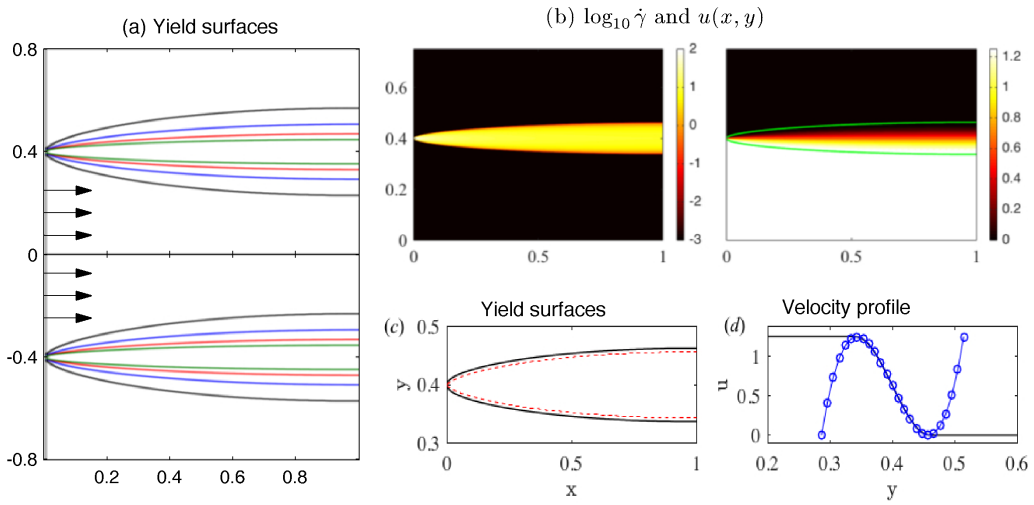

Figure 14: Oldroyd's jet with its two shear layers. (a) shows yield surfaces for $B = 32$, 128, 512 and 2048. (b) shows $\log_{10}\dot{\gamma}$ and u as densities on the $(x, y)-$plane (half of the jet is shown), with the yield surfaces indicated, for $B = 20148$. (c) and (d) compare the yield surfaces and horizontal velocity profile of the upper shear layer with the prediction of the self-similar boundary layer solution (dotted red line and blue line with circles).

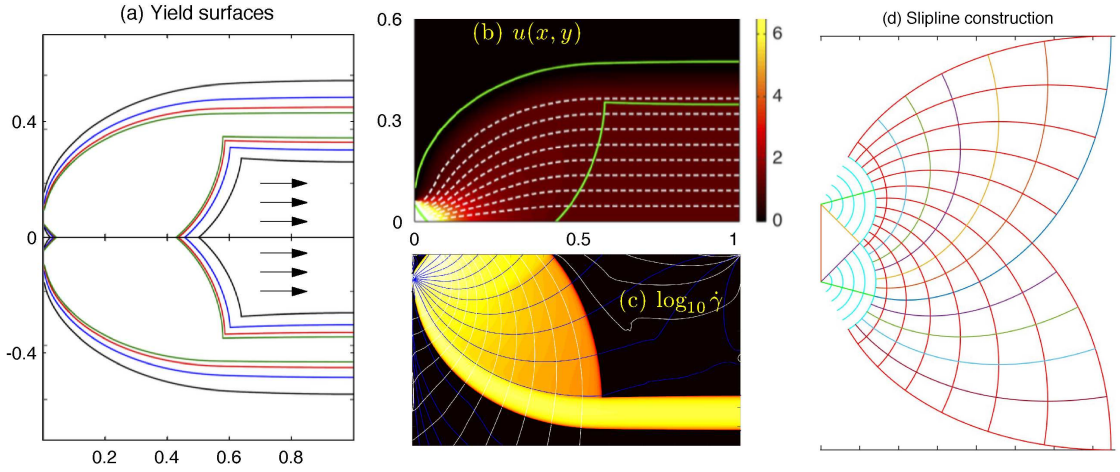

Figure 15: A narrower jet. Again (a) shows the yield surfaces for $B = 32$, 128, 512 and 2048. (b) shows u, the yield surfaces and sample streamlines for $B = 2048$. (c) shows $\log_{10}\dot{\gamma}$ along with a selection of sliplines, as reconstructed from p and $\vartheta = -\frac{1}{2}\tan^{-1}(\sigma/\tau)$. (d) shows a slipline construction directly from the characteristic equations, beginning from two expansion fans and demanding that the sliplines meet at fortyfive degrees along the symmetry line.

arcs (this follows from Hencky's rules, that dictate the geometry of the slipline field [36]). Further from the centre of the fans, the outgoing sliplines begin to curve so that the other

slipline family meets the symmetry line at the required angle. The slipline field must now be constructed by integrating the slipline equations. In principle, this direct construction of the slipline field offers a means to predict the emergent jet thickness.

Oldroyd's second problem studied the boundary layer around a knife or plate pushed through an infinite Bingham fluid (see figure 13(b)). This configuration has recently been the focus of an experimental study [13], which claims that one needs to supplement the viscoplastic boundary-layer solution with elastic-type deformation within the plug zones to generate a complete solution for the flow field. A computation of the steady flow around a finite plate is shown in figure 16. In this purely Bingham computation, the flow takes a boundary-layer form against the plate, as found experimentally and suggested by Oldroyd. The scaling of this boundary layer is not $B^{-1/3}$, however, but $B^{-1/2}$. In addition, fluid also circulates around to either side of the plate in two rigidly rotating vortices with diameter comparable to the length of the plate. The rigid rotation is bordered by a circular shear layer whose structure is actually of the Oldroyd $B^{-1/3}-$type. Besides the vortices and boundary layers, there are also regions of nearly plastic flow at the leading and trailing edges of the plate. The sliplines over those regions contain expansion fans centred at the plate's end and a network emerging from the viscoplastic boundary layer along the plate somewhat like Prandtl's construction (figure 8). The two are stitched together by a stress discontinuity, which is permissible in ideal plasticity if the tangential stress is discontinuous but the normal stress is continuous. Overall, the flow structure is quite different from Oldroyd's expectations, but matches solutions found for flow around elongated ellipses and rectangles (E. Chaparian, *in preparation*). Having said that, it is not so clear how one could extrapolate this solution to Oldroyd's semi-infinite knife.

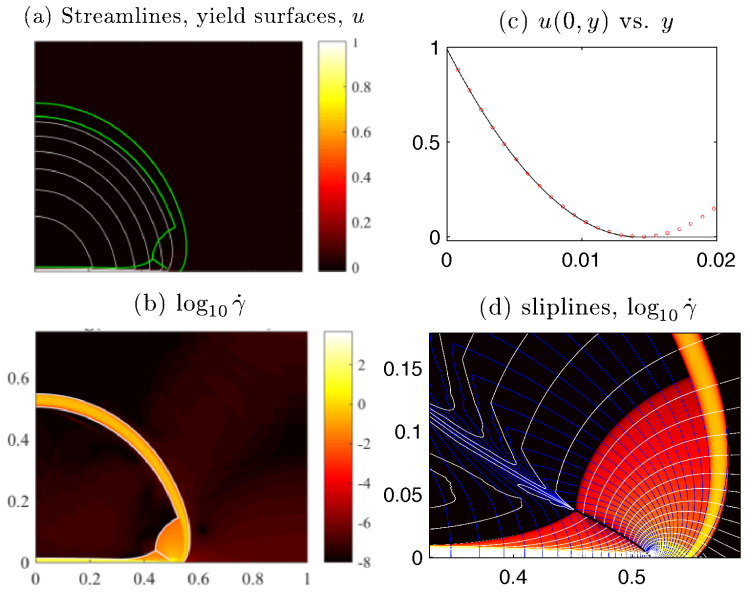

Figure 16: Oldroyd's moving plate, showing the solution in the first quadrant; the plate occupies $-\frac{1}{2} < x < \frac{1}{2}$ and $y = 0$. (a) and (b) show u and $\log_{10}\dot\gamma$ as densities on the $(x, y)-$plane. (a) includes the yield surfaces and a selection of streamlines. (c) compares the boundary-layer velocity profile $u(0, y)$ with the asymptotic prediction in (75), taking Y from the numerical solution. (d) shows a magnification of the plastic region, with a reconstruction of the slipline field overlaid on a density map of $\log_{10}\dot\gamma$. $B = 2048$.

Difficulties with the boundary-layer theory of §3.1–3.2 for the plate problem were already pointed out by Oldroyd: instead of imposing a symmetry condition at $\zeta = 0$, as for the shear layer, one must impose no-slip: $U(x, 0) = V(x, 0) = 0$. One must also match the boundary-

layer solution to a plug or plastic flow outside the boundary layer, which corresponds to demanding that U, U_ζ and V should all become small at $\zeta = Y$. But the two conditions on $V(x,\zeta)$ cannot both be satisfied in Oldroyd's theory because V follows from integrating the continuity equation, $V_\zeta = -U_x$, which is only first order in ζ. Instead, Oldroyd proposed that one should impose $V(x,0) = 0$ and omit the other boundary condition, suggesting that the nonvanishing transverse velocity at the edge of the boundary layer could be accounted for by allowing a modest elastic deformation over the region outside the boundary layer. Evidently, however, the core of the problem is that the boundary-layer scaling is not $B^{-1/3}$.

The narrower $B^{-1/2}$ boundary layer is analogous to the large B limit of the fully yielded regions in lubrication theory (*cf.* (40)). For the flow around the plate, the appropriate scalings and main balances are

$$p = \frac{P(x,\eta)}{\varepsilon^2}, \quad \tau = -B + \frac{1}{\varepsilon}u_\zeta + ..., \quad P_x = u_{\zeta\zeta} \quad \& \quad P_\zeta = 0. \tag{74}$$

The link between the boundary layer thickness ε and B does not follow from the force balance equations here. Instead, one must argue that $\varepsilon = B^{-1/2}$ is demanded by matching the boundary-layer solution with the other regions in the flow. In particular, over the plastic region at the front and back of the plate, we must have $p = O(B)$ for a non-trivial slipline solution (see §2.6). Given $u(x,0) = 1$ (the velocity of the plate), equations (74) predict the parabolic velocity profile,

$$u = \left[1 - \frac{\zeta}{Y(x)}\right]^2, \tag{75}$$

where $\zeta = Y = \sqrt{2P_x}$ now denotes where the boundary layer meets either the rigid rotation or the plastic flow (where u and u_ζ become small; *cf.* figure 16).

Piau [34] has also considered $B^{-1/2}$ boundary layers around the plate in a revision of Oldroyd's original analysis. Despite the different balances that this alternative scaling implicitly implies, Piau (somewhat obscurely) analyses the problem in a non-asymptotic fashion, keeping both the leading order and some of the correction terms. Instead of the simple equations outlined above (and their equally straightforward solution), he then arrives at Oldroyd's boundary-layer equations and writes down another self-similar solution. None of this elabouration appears necessary, although in some situations, retaining additional correction terms along with the leading order can improve an asymptotic solution (*cf.* §4.4).

For a third example, we consider channel flow through an expansion, as considered experimentally by Chevalier *et al.* [16], and who argued this to be a canonical viscoplastic analogue of the shear-banding of plastic materials in "frustrated flows" (Chevalier *et al.* considered pipe flow; we continue with the two-dimensional problem here). In the limit of large yield stress, the flow down the uniform part of the channel is largely plug-like, lubricated by thin boundary layers. When the plug meets the expansion, slightly less narrow shear layers develop to isolate the moving plug from rigid fluid in the clogged-up expansion. Figure 17 shows a computation of the configuration (assumed periodic, and again using the Augmented Lagrangian algorithm). The free shear layers have the $B^{-1/3}-$scaling and are well described by Oldroyd's boundary-layer analysis and similarity solution; the boundary layers against the channel walls, on the other hand, follow the $B^{-1/2}$ scaling.

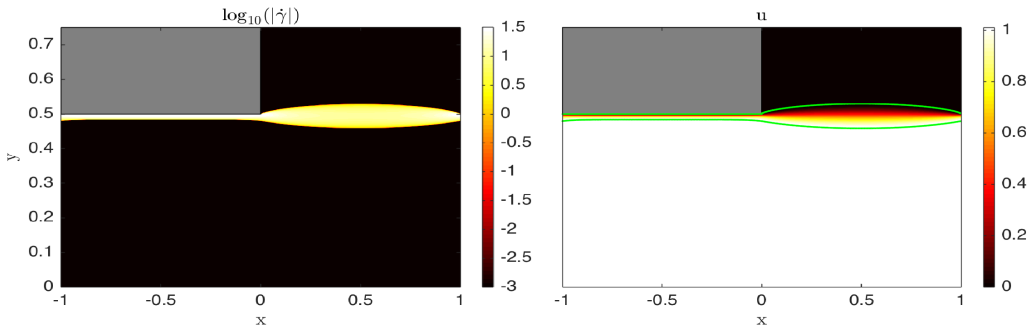

Figure 17: Channel flow past a rectangular expansion at $B = 2048$, showing density maps of $\log_{10}\dot{\gamma}$ and u. The upper half of the solution is displayed. Plugs are shaded black; grey shows the bounding wall.

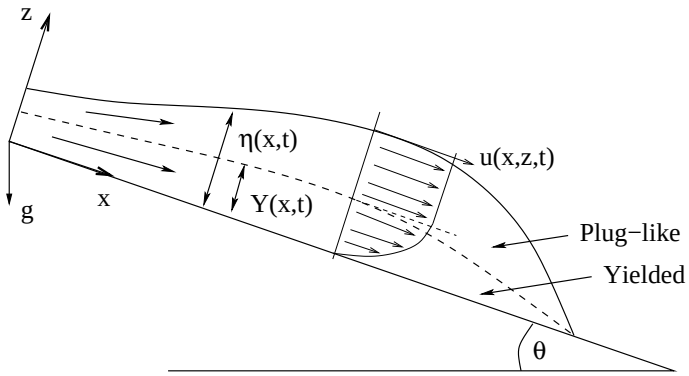

Figure 18: Sketch of the geometry for a sticky viscoplastic film flow.

4 Free-surface flow

We now consider a different range of problems, introducing gravity and endowing our thin layers of viscoplastic fluid with a free surface.

4.1 Sticky viscoplastic films

Returning to the lubrication model of §2, we consider the gravity-driven flow of a film of Bingham fluid over an inclined planar surface. We align an $(x, z)-$Cartesian coordinate system with the inclined plane, with x pointing down slope. The free surface lies at $z = \eta(x, t)$. See figure 18. The dimensional thin-film equations are

$$u_x + w_z = 0, \quad p_x = \tau_z + \rho g \sin\theta, \quad \& \quad p_z = -\rho g \cos\theta, \tag{76}$$

where g is gravity, ρ the fluid density and θ the angle of inclination with respect to the horizontal. With the scalings

$$x = \mathcal{L}\hat{x}, \quad (z, \eta) = \mathcal{H}(\hat{z}, \hat{\eta}), \quad (u, w) = \mathcal{U}(\hat{u}, \epsilon\hat{w}), \quad (p, \tau, \sigma) = \frac{\mu\mathcal{U}\mathcal{L}}{\mathcal{H}^2}(\hat{p}, \epsilon\hat{\tau}, \epsilon\hat{\sigma}), \tag{77}$$

and after dropping the hat decoration, we convert the force balance equations into the dimensionless form,

$$p_x = \tau_z + \mathrm{G_x}, \quad \& \quad p_z = -\mathrm{G_z}, \tag{78}$$

where the gravity parameters $\mathrm{G_x} = \rho g \mathcal{H}^3 \cos\theta/(\mu \mathcal{U}\mathcal{L})$ and $\mathrm{G_z} = \rho g \mathcal{H}^3 \cos\theta/(\epsilon \mu \mathcal{U}\mathcal{L})$, both of which are assumed to be order one, which requires that the slope is relatively shallow. The Bingham law implies

$$\tau = u_z + B \ \mathrm{sgn}\ (u_z) \ \text{if} \ |\tau| > B, \tag{79}$$

and $u_z = 0$ otherwise, where $B = \tau_Y \mathcal{L}/(\rho g \mathcal{H}^2)$. At the free surface of the film, the thin-film scalings implies the stress conditions,

$$p(z, \eta, t) = \Pi(x, t) - \Gamma \eta_{xx} \qquad \& \qquad \tau(x, \eta, t) = 0, \tag{80}$$

where $\Gamma = \gamma \mathcal{H}^3/(\mu \mathcal{U}\mathcal{L}^3)$ is an inverse Capillary number and the normal surface force Π accounts for the ambient pressure of an overlying (inviscid) fluid such as air or water (*cf.* I. Wilson's lectures on cleaing and fouling). The kinematic condition demands

$$\eta_t + u(x, \eta, t)\eta_x = w(x, \eta, t). \tag{81}$$

It now follows that the pressure distribution is hydrostatic,

$$p = P - \mathrm{G_x} z \equiv \Pi - \Gamma \eta_{xx} + \mathrm{G_x}(\eta - z) \tag{82}$$

(P being the base pressure), and related to the shear stress by

$$\tau = (\mathrm{G_x} - P_x)(\eta - z) = (\mathrm{G_x} - \mathrm{G_z}\eta_x - \Pi_x + \Gamma \eta_{xxx})(\eta - z). \tag{83}$$

The velocity profile is

$$u = \tfrac{1}{2}(\mathrm{G_x} - P_x) \times \begin{cases} z(2Y - z), & 0 < z < Y, \\ Y^2, & Y < z < \eta, \end{cases} \qquad Y = \mathrm{Max}\left(0, \eta - \frac{B}{|\mathrm{G_x} - P_x|}\right), \tag{84}$$

if there is no slip on the inclined plane ($u = w = 0$ on $z = 0$). The region $Y < z < \eta$ is occupied by a pseudo-plug (figure 18).

Finally, given the $z-$integrated mass conservation equation,

$$\frac{\partial \eta}{\partial t} + \frac{\partial}{\partial x} \int_0^\eta u \ \mathrm{d}z = 0, \tag{85}$$

we find the evolution equation for the fluid depth,

$$\frac{\partial \eta}{\partial t} = \frac{\partial}{\partial x}\left[\frac{1}{6}(3\eta - Y)Y^2(P_x - \mathrm{G_x})\right]. \tag{86}$$

Without surface pressure variations and tension ($\Gamma = \Pi_x = 0$) this equation and some of its generalizations are reviewed in [4] (a first derivation being given by [28]).

The main feature of the model that we point out here is that fluid yields and spreads provided $Y > 0$. Hence, when $Y \to 0$, flow must come to a halt, furnishing an equation for a slumped deposit:

$$|\mathrm{G_x} - P_x|\eta = B. \tag{87}$$

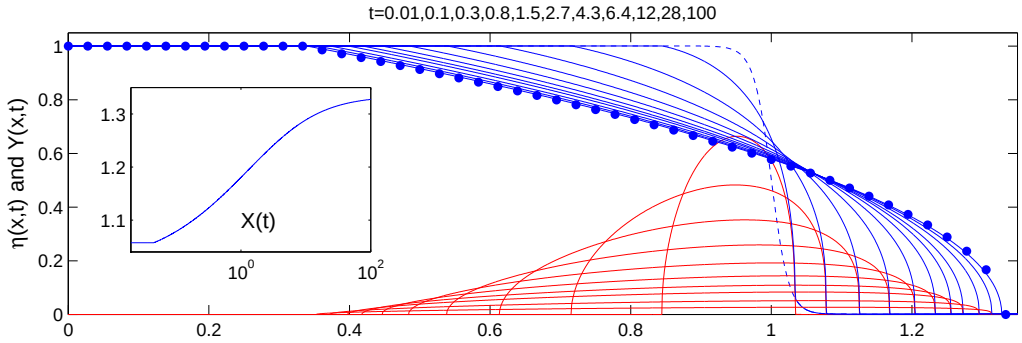

Figure 19: Spreading viscoplastic current with $B = 0.5$, $\mathrm{G_z} = 1$, $\mathrm{G_x} = 0$, $\Gamma = 0$ and $\Pi = 0$, starting from a smoothed dambreak configuration that includes a pre-wetted film of thickness 10^{-3} to ease the computation and avoid a true contact line ($\eta(x,0) = \frac{1}{2}[1 - \tanh 20(x^2 - 1)] + 10^{-3}$; dashed line). Shown are snapshots of $\eta(x,t)$ and $Y(x,t)$ at the times indicated; the dots show the final shape from (88). The solution is symmetrical about $x = 0$ and only the half in $x > 0$ is plotted. The inset shows the evolution of the front of the current $X(t)$.

On a flat surface and omitting surface tension and pressure variations ($\mathrm{G_x} = \Gamma = \Pi = 0$), we then find (*cf.* [30]).

$$\eta = \sqrt{1 - 2\mathrm{G_z}^{-1} B|x|}, \tag{88}$$

if we choose $\mathcal{H}$ as the maximum depth, and after shifting the position of the maximum to $x = 0$. The progress to this state is illustrated in figure 19, which shows a numerical solution to (86), starting from a dambreak-type configuration (an initial-value problem that is relevant to the "Bostwick consistometer," a practical rheometer used in food science [3]).

A numerical solution that includes surface tension ($\Gamma \neq 0$) is shown in figure 20. In this case, once the fluid is released, the high curvature of the initial state generates a rapid adjustment in which a prominent ridge and capillary wave train propagate towards the centre of the fluid, yielding the fluid layer en route. Flow eventually subsides, as in figure 19, but with the entire initial reservoir having collapsed. Again the final state is predicted by (87), which for the current parameter settings becomes

$$\Gamma \eta_{xxx} - \mathrm{G_x} \eta_x = \frac{B}{\eta}, \tag{89}$$

assuming $P_x < 0$ and the boundary conditions $\eta(X) = \eta'(X) = 0$ at the fluid edge $x = X$ (some care needs to be taken in arriving at this boundary condition; Jalaal, Balmforth & Stoeber, *in preparation*).

The model in (86) is analogous to that used for viscous gravity currents [18]. As in that Newtonian problem, rather elabourate machinations are required to add inertia to the theory [20]. This arises because the $z-$dependence of the velocity field forbids a simple approximation of the inertial terms and also changes with their introduction. Perhaps the most significant extension of the viscoplastic film theory for the future is to explore the inertial generalization of the model.

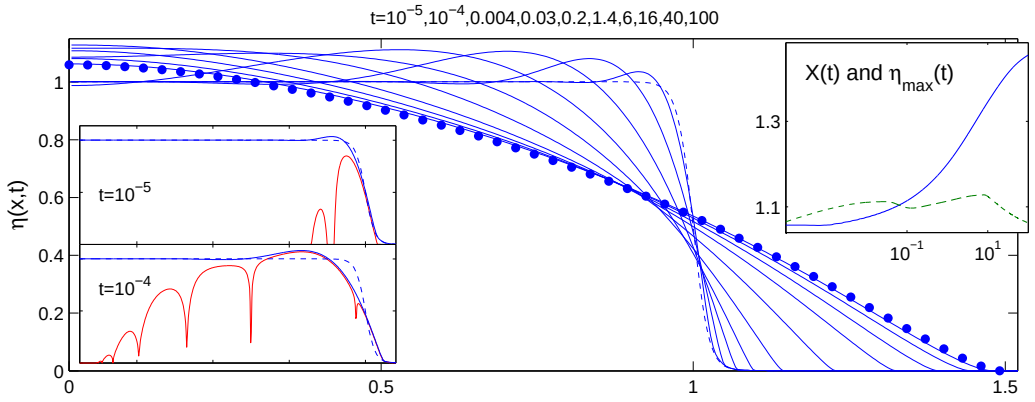

Figure 20: Dambreak with $B = 0.5$ and $\Gamma = 0.1$ ($\mathrm{G_z} = 1$, $\mathrm{G_x} = \Pi = 0$; $\eta(x,0) = \frac{1}{2}[1 - \tanh 20(x^2 - 1)] + 10^{-3}$). Shown are snapshots of $\eta(x,t)$ at the times indicated; the dots show the final shape expected from (89). The insets show the evolution of the front of the current $X(t)$ and its maximum depth $\eta_{max}(t)$, and the two earliest snapshots including $Y(x,t)$.

4.2 Sliding films

What happens when the condition on the base of the film is not no-slip? In some geophysical problems, like glacier flow, this is a very real consideration in view of the physical condition of the interface between ice and the underlying terrain and the lubricating action of any water [40]. For many non-Newtonian fluids in engineering this is also important because of the tendency for these materials to suffer apparent slip (*e.g.* [8]; lectures by I. Wilson). Indeed, slip has been observed directly in drops of viscoplastic fluid spreading over glass surfaces [26]. Nevertheless, despite the widespread its occurence, physical models of slip are rare and slip laws are mostly based on empiricism.

To consider the effect of slip on the film model above, we abandon the no slip condition in favour of a relation between the basal shear stress, $\tau_b \equiv \eta(\mathrm{G_x} - \eta_x)$, and slip velocity u_s. In particular, we take

$$u_s = k\ \mathrm{Max}(0, |\tau_b| - B_w)^m\ \mathrm{sgn}(\tau_b), \tag{90}$$

with (suitably scaled) dimensionless parameters k, B_w and m. A simple power-law of the form, $u_s = k|\tau_b|^m\ \mathrm{sgn}(\tau_b)$, for the slip law has the unappealing feature that material would slide over the bounding surface however small the basal stress, in contrast to the everyday observation that drops of viscoplastic fluid do adhere to shallowly inclined surfaces without flowing or sliding. The inclusion of B_w accounts for a sliding threshold.

With the sliding law in (90), spreading will either not occur at all if $|\tau_b| < (B_w, B)$, via sliding alone if $B_w < |\tau_b| < B$, through internal shear flow with no slip if $B < |\tau_b| < B_w$, or both shear and slip if $|\tau_b| > (B, B_w)$. In most situations one expects that $B_w < B$. Motion will then halt only after sliding ceases for $\tau_b = |\mathrm{G_x} - P_x|\eta \to B_w$, which predicts the same final shapes as above save that B is replaced by B_w. Hence in spreading tests, there is a danger that one might incorrectly diagnose the yield stress from the sliding threshold.

The final phase of spreading (with $B_w < |\tau_b| < B$) is controlled purely by the basal

friction from the slip layer; the overlying flow is plug-like with $u = u_s$ and the analogue of (86) is

$$\frac{\partial \eta}{\partial t} = -\frac{\partial}{\partial x}\left(\eta u_s\right) = -k\frac{\partial}{\partial x}\left[\eta Y_w^m |P_x - \mathrm{G_x}|^{m-1}(P_x - \mathrm{G_x})\right], \qquad Y_w = \eta - \frac{B_w}{|\mathrm{G_x} - P_x|}. \quad (91)$$

Evidently, the dynamics appears to be independent of the bulk rheology, although the spreading fluid cannot be rigid (u_s will in general depend on x). In fact, the whole layer is a pseudo-plug due to its yield stress.

4.3 Viscoplastic membrane models

A curious feature of the sliding film model is that the basal friction controls spreading and the only role of the bulk fluid rheology is to suppress shear and establish the pseudo-plug. If the underlying surface is very slippy, however, this is unrealistic as one expects that extensional stresses in the plane of the film ought to limit the spreading of the fluid. Above, such stresses have been omitted from the main balance of forces; to restore them, a different set of scalings is needed. The point is that the relatively free sliding of the fluid layer relieves the shear stress sufficiently to enhance the extensional stresses. We therefore introduce

$$(p, \tau, \sigma) = \frac{\mu\mathcal{U}}{\mathcal{L}}(\hat{p}, \epsilon\hat{\tau}, \hat{\sigma}), \quad (92)$$

to furnish the force balance equations

$$p_x = \sigma_x + \tau_z + \mathrm{G_x}, \quad \& \quad p_z + \sigma_z = -\mathrm{G_z}, \quad (93)$$

where we redefine the gravity parameterz as $(\mathrm{G_x}, \mathrm{G_z}) = \rho g\mathcal{L}^3(\epsilon^{-1}\sin\theta, \cos\theta)/(\mu\mathcal{U})$. The stress conditions at the surface must also be revised:

$$p(z, \eta, t) + \sigma(x, \eta, t) = \Pi(x, t) - \Gamma\eta_{xx} \qquad \& \qquad \tau(x, \eta, t) - 2\eta_x\sigma(x, \eta, t) = 0, \quad (94)$$

with $\Gamma = \gamma\mathcal{H}/(\mu\mathcal{U}\mathcal{L})$. Thus, integrating both relations in (93) in z,

$$p + \sigma = \Pi + \eta - z \qquad \& \qquad 0 = \eta(\mathrm{G_x} - \mathrm{G_z}\eta_x - \Pi_x + \Gamma\eta_{xxx}) - \tau_b + 2\frac{\partial}{\partial x}\int_0^\eta \sigma \mathrm{d}z, \quad (95)$$

in which we see the emergence in importance of the extensional stress σ.

Despite the satisfying balances in (95), there is an apparent inconsistency with the constitutive law which indicates that $(\sigma, \epsilon\tau) \propto (2u_x, \epsilon^{-1}u_z)$ in view of (92). However, we now operate in the limit that sliding is relatively free, and so we cannot expect that much shear builds up in u. We therefore set

$$\dot{\gamma} = 2\left|\frac{\partial u_s}{\partial x}\right| + O(\epsilon^2), \qquad u = u_s(x, t) + \epsilon^2 u_2(x, z, t), \qquad w = -z\frac{\partial u_s}{\partial x} + O(\epsilon^2), \quad (96)$$

and

$$(\sigma, \tau) = \left(1 + \frac{B}{\dot{\gamma}}\right)\left(2\frac{\partial u_s}{\partial x}, \frac{\partial u_2}{\partial z}\right), \qquad \text{if } |\sigma| > B, \quad (97)$$

and $\partial u_s/\partial x = 0$ otherwise, where $B = \tau_Y \mathcal{L}/(\mu \mathcal{U})$.

At this stage, computing the correction u_2 is not needed and we arrive the paired evolution equations,

$$\eta_t + (\eta u)_x = 0 \qquad \& \qquad \mathrm{Re}\,(u_t + u u_x) = \mathrm{G_x} - \mathrm{G_z}\eta_x - \Pi_x + \Gamma \eta_{xxx} - \frac{1}{\eta}\tau_b + \frac{2}{\eta}\frac{\partial}{\partial x}(\eta\sigma), \quad (98)$$

given $u \approx u_s$ and where we have also restored the leading-order inertial terms with Reynolds number $\mathrm{Re} = \rho \mathcal{U} \mathcal{L}/\mu$, which is acceptable in our asymptotic scheme in view of the plug-like character of the flow (unlike in §4.1). We may also immediately generalize to the Herschel-Bulkley version of the model by writing

$$\sigma = 2u_x \left(|2u_x|^{n-1} + \frac{B}{2|u_x|} \right) \quad \text{for } |\sigma| > 0 \quad \& \quad u_x = 0 \text{ otherwise} \qquad (99)$$

(though we consider only the Bingham case, $n = 1$, in all examples).

The model in (98)–(99) is what one might call a membrane model in solid mechanics [29]. In fluid dynamics, the model is equivalent to that for free viscous films and jets [18], Savage-Hutter-like models for granular flows [7], fast-moving ice streams and floating ice shelves (with $\mathrm{Re} \to 0$) [40], and viscoplastic threads [5]. Indeed, by dropping the basal drag τ_b, the model becomes identical to that for the evolution of a viscoplastic jet under varicose disturbances (perturbations symmetric about the midline), with $\eta(x,t)$ re-interpreted as the half-thickness.

To reconsider the gravitational spreading problem of §4.1-4.2, we set $\mathrm{Re} = \Gamma = \Pi_x = 0$ and take (90) for τ_b. Assuming that the fluid approaches rest with $(u, u_x) \to 0$ and $\mathrm{sgn}(u_x) = s = \pm 1$, the final shape is dictated by balancing the remaining terms the momentum equation in (98): given that $\sigma \to sB$ and $|\tau_b| \to B_w$ these terms combine into the relation,

$$|(2sB - \eta \mathrm{G_z})\eta_x - \eta \mathrm{G_x}| = B_w. \qquad (100)$$

To examine the shape this predicts in more detail, we consider a flat plane ($\mathrm{G_x} = 0$). If the centre of the drop, with $\eta = \eta_{max}$, is at $x = 0$, $\eta_x < 0$ and $\eta - sB > 0$ just to the right. Thence

$$\eta = \sqrt{(\eta_{max} - 2s\mathrm{G_z}^{-1}B)^2 - 2\mathrm{G_z}^{-1}B_w x} + 2s\mathrm{G_z}^{-1}B. \qquad (101)$$

For a flow in compression ($s < 0$), this profile can decrease to zero, with finite slope at the edge. On the other hand, when the flow comes to rest in expansion ($s > 0$), the solution must terminate at a finite height to avoid becoming multi-valued. This suggests either that the edge is vertical (in violation of the slender asymptotics) or that a rim of unyielded fluid borders the main body of the slumped current.

Sample numerical solutions to (98) are shown in figure 21, and again correspond to dam-break-like initial-value problems (with neither surface pressure variation nor tension, $\Pi = \Gamma = 0$). The first example includes both an extensional yield stress and bottom drag with a finite threshold; no drag is included for the second case. Both slide to a halt with a shape given by (101). The flows are in extension, and the final shapes terminate in abrupt cliffs of unyielded fluid that were pushed ahead of the extending current.

The second example of figure 21 spreads out with a distinctive flat-topped profile, revealing how an analytical solution of the problem is feasible in this case: although the Reynolds

number used for the computation is $\mathrm{Re} = 1$, the velocity u remains small throughout. In this situation, the inertial terms are small and over the bulk of the current one may take the solution,

$$\eta = N(t) \qquad \& \qquad u = x\Upsilon(t), \tag{102}$$

with (from the first relation in (98))

$$\frac{\mathrm{d}N}{\mathrm{d}t} + \Upsilon N = 0. \tag{103}$$

This spatial profile must be terminated by a jump or shock at the flow front, $x = X(t)$. Two further relations then follow from imposing the jump conditions,[3]

$$\frac{\mathrm{d}X}{\mathrm{d}t} = -\Upsilon X \qquad \& \qquad \tfrac{1}{2}\mathrm{G_z} N = 2\sigma \equiv 4\Upsilon + 2B. \tag{104}$$

Thus, $NX = 1$ if $N(0) = X(0) = 1$ (an obvious demand of mass conservation) and

$$\frac{\mathrm{d}N}{\mathrm{d}t} = -\frac{1}{8}N(N - 4B), \qquad \text{or} \qquad N = 4B\left[1 - (1 - 4B)e^{-Bt/2}\right]^{-1}, \tag{105}$$

if $\mathrm{G_z} = 1$. This solution, which is compared to the numerical computation in figure 21, exposes the final state, $\eta \to 4B$, and yield condition, $4B < 1$. The latter is characteristic of the initial condition and arises because the jump in the net hydrostatic pressure at the edge of the fluid can be balanced by the extensional stress 2σ without failure provided σ does not exceed the yield stress. When the initial extensional stress exceeds B, sliding ensues, until the extension of the layer reduces the net hydrostatic pressure on the side face to the equilibrium level $4B$. Much that same happens when $B_s \neq 0$ although that threshold affects both the failure condition and final rest state.

4.4 Jet instability

To explore the (varicose) instability of a high-speed viscoplastic jet in air, we need a prescription for the dynamic pressure due to the irrotational flow of ambient air. For this, we need to solve Laplace's equation for the velocity potential $\mathcal{UH}\phi(x, y, t)$ (with y scaled

[3]The first shock condition (Rankine-Hugoniot relation [47]) follows from first writing the mass-conservation equation in (98) as a integral conservation law,

$$0 = \frac{\mathrm{d}}{\mathrm{d}t}\int_{x_1}^{x_2} \eta(x,t)\mathrm{d}x + [J(x,t)]_{x=x_1}^{x=x_2} = \int_{x_1}^{X} \eta_t(x,t)\mathrm{d}x + \int_{X}^{x_2} \eta_t(x,t)\mathrm{d}x + \Big[J(x,t) - \dot{X}\eta(x,t)\Big]_{x=x_1}^{x=x_2},$$

where $J = hu$ is the mass flux, x_1 and x_2 are arbitrary locations straddling the shock, and $X^{\pm}$ implies the limit from either the left or right. By taking $x_1 \to X^-$ and $x_2 \to X^+$ and arguing that the remaining integrals then become negligible, we then find

$$\dot{X}\,[\eta(x,t)]_{x=X^-}^{x=X^+} = [J(x,t)]_{x=X^-}^{x=X^+}.$$

The second relation follows from applying the same argument to the momentum equation in (98) ($\Gamma = 0$):

$$\dot{X}\mathrm{Re}\,[\eta u]_{x=X^-}^{x=X^+} = \left[\mathrm{Re}\,\eta u^2 - 2\eta\sigma + \tfrac{1}{2}\mathrm{G_z}\eta^2\right]_{x=X^-}^{x=X^+}.$$

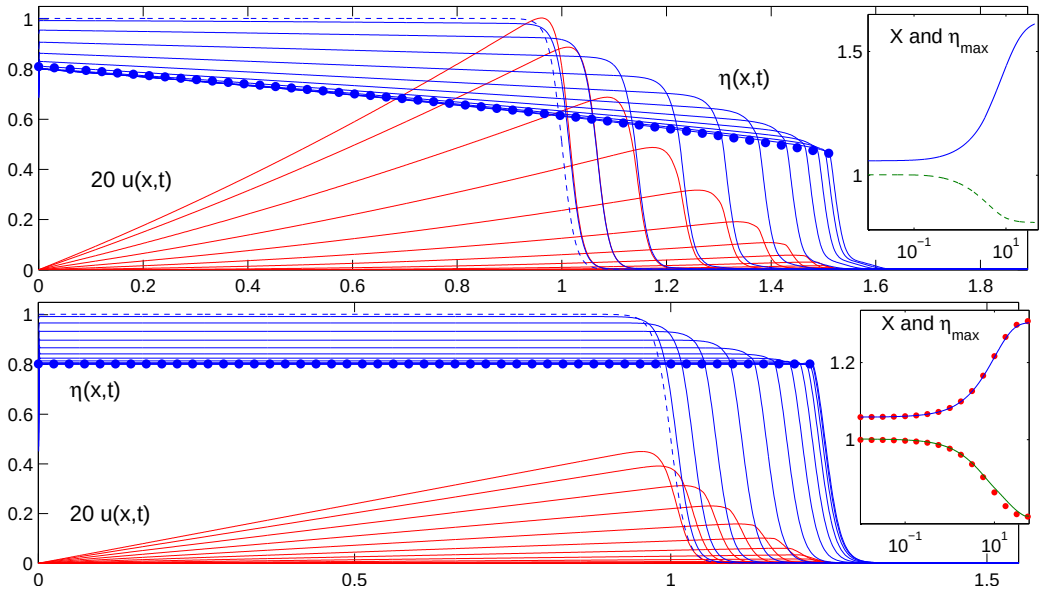

Figure 21: Dambreak of a sliding viscoplastic current with (a) $B = 0.1$, $B_s = 0.1$, $m = 1$ and $k = 1$, and (b) $B = 0.2$ and $B_s = k = 0$. Both have $\mathrm{Re} = \mathrm{G_z} = 1$, $\mathrm{G_x} = \Gamma = \Pi = 0$, $u(x,0) = 0$ and $\eta(x,0) = \frac{1}{2}[1 - \tanh 20(x^2 - 1)] + 10^{-3}$ (dashed line). Shown are snapshots of $\eta(x,t)$ and $u(x,t)$ at $t = j^2/5$, $j = 1, 2, ..., 12$. The dots show the final shape from (101) given the final maximum depth η_{max}. The insets show the evolution of the front of the current $X(t)$ and $\eta_{max}(t)$; in (b), the dots show the prediction in (105), with the starting value of X adjusted to account for the finite thickness of the front (*i.e.* $X = 1/N + X(0) - 1$).

with $\mathcal{L}$ rather than the film thickness) subject to the boundary conditions on the fluid-air interface. Those conditions are

$$\phi_y(x,0,t) = \eta_t + O(\epsilon) \qquad \& \qquad \frac{\partial}{\partial x}\left[\epsilon\varrho \mathrm{Re}\phi_t(x,0,t) + p_a\right] = O(\epsilon^2), \tag{106}$$

where ϱ is the ratio of air to fluid density, p_a is the interfacial air pressure (scaled by $\mu\mathcal{U}/\mathcal{L}^2$), which follow from the leading order kinematic condition and Bernoulli's law. The last of these relations indicates that the air pressure contribution to Π if $O(\epsilon)$ if $\varrho\mathrm{Re} = O(1)$; we keep this correction term along with the leading order in view of the fact that it is the source of instability. Further justification can be given from the observation that all the corrections to (98) are $O(\epsilon^2)$. It is therefore consistent to include an $O(\epsilon)$ approximation to p_a.

Laplace's equation can be solved using the Fourier transform [43]: if we denote the transform of $f(x)$ and its inverse by

$$\check{f}(k) = \mathcal{F}\{f(x)\} = \int_{-\infty}^{\infty} f(x)e^{-ikx}\mathrm{d}x \qquad \& \qquad f(x) = \mathcal{F}^{-1}\{\check{f}(k)\} = \int_{-\infty}^{\infty} \check{f}(k)e^{ikx}\frac{\mathrm{d}k}{2\pi}, \tag{107}$$

then one can verify that $\check{\phi}(k,y,t) = e^{-|k|y}\check{\phi}(k,0,t)$. The conditions in (106) now imply

$$-|k|\check{\phi}(k,0,t) = \mathcal{F}\{\eta_t\} \qquad \& \qquad ik\epsilon\varrho\mathrm{Re}\check{\phi}_t(k,0,t) + \mathcal{F}\{\partial p_a/\partial x\} = 0. \tag{108}$$

Hence

$$\frac{\partial}{\partial x}p_a = \epsilon\varrho\mathrm{Re}\; y\mathcal{F}^{-1}\left\{i\;\mathrm{sgn}(k)\mathcal{F}\{\eta_{tt}\}\right\} \equiv -\epsilon\varrho\mathrm{Re}\;\mathrm{H}\{\eta_{tt}\}, \tag{109}$$

where

$$\mathrm{H}\{f(x)\} = \frac{1}{\pi}\fint \frac{f(z)\,\mathrm{d}z}{x-z} \tag{110}$$

is the Hilbert transform [43] (and the extra decoration on the integral symbol indicates that the principal value must be taken to render the integral non-singular).

Now consider the stability of a viscoplastic jet, ignoring gravity $\mathrm{G_x} = \mathrm{G_z} = 0$ and basal drag $\tau_b = 0$. The evolution equations become

$$\eta_t + (\eta u)_x = 0 \qquad \& \qquad \mathrm{Re}\,(u_t + uu_x) = \epsilon\varrho\mathrm{Re}\;\mathrm{H}\{\eta_{tt}\} + \Gamma\eta_{xxx} + \frac{2}{\eta}\frac{\partial}{\partial x}(\eta\sigma). \tag{111}$$

For a Newtonian jet, it is straightforward to consider the stability of small perturbations about the uniform equilibrium $u = \eta = 1$ with dependence $\exp ik(x-ct)$, where k is the wavenumber and c the (complex) wavespeed. One can thereby establish that perturbations are unstable for $k < \epsilon\varrho\mathrm{Re}/\Gamma$, and one expects these modes to grow to break up the jet.[4] For a Bingham fluid, on the other hand, the equilibrium is unconditionally stable because the stress of the basic state, $\sigma = 0$, is finitely below the yield stress B. Thus, the jet can only break up given a finite-amplitude initial perturbation. The situation is closely related to the removal of the Rayleigh instability in viscoplastic threads with surface tension [5] and mirrors many other viscoplastic problems of hydrodynamic stability (see lectures by I. Frigaard and S. Hormozi).

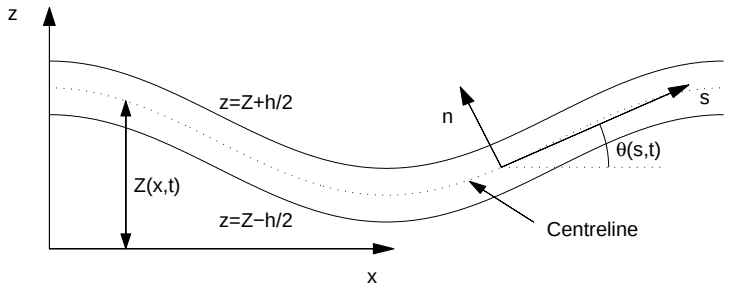

Figure 22: Sketch of the geometry for a viscoplastic beam.

4.5 Viscoplastic beams

When the fluid is not stuck down to an underlying surface, it can become easier for the viscoplastic film to buckle out of plane rather than deform symmetrically with respect to the midline (figure 22). This calls for a different development of the thin-layer equations [6]. We begin with the scaling of the stress components:

$$(p, \tau, \sigma) = \frac{\mu\mathcal{U}\mathcal{H}}{\mathcal{L}^2}(\hat{p}, \epsilon\hat{\tau}, \hat{\sigma}), \tag{112}$$

[4]The restriction to varicose perturbations ignores the (very real) possibility that sinuous perturbations may be more unstable and dominate the break-up dynamics. Sinuous perturbations require a consideration of the bending of the midline of the fluid layer, along the lines considered in §4.5.

but add the further constraint $-p-\sigma=\epsilon^2 s_{zz}$. That is, $p=-\sigma+O(\epsilon^2)$, which reduces the normal stress in the $z-$direction to $O(\epsilon^2)$, thereby achieving the force balances,

$$p_x=\sigma_x+\tau_z+\mathrm{G_x}, \quad \& \quad 0=\tau_x+\frac{\partial}{\partial z}s_{zz}-\mathrm{G_z}, \tag{113}$$

with the gravity parameters, $(\mathrm{G_x},\mathrm{G_z})=\rho g\mathcal{L}^2(\sin\theta,\epsilon^{-1}\cos\theta)/(\mu\mathcal{U}\mathcal{H})$, so the film is now either nearly vertical ($\theta\approx\frac{1}{2}\pi$; $\epsilon^{-1}\cos\theta)=O(1)$) or horizontal ($\mathrm{G_z}=O(1)$ and $\mathrm{G_x}\to 0$).

We place the surfaces at $z=\eta_\pm(x,t)=Z(x,t)\pm\frac{1}{2}h(x,t)$, where $z=Z(x,t)$ is the midline of the sheet, and ignore surface pressure variations and tension. The surface stress conditions are then

$$s_{zz}-\eta_x\tau=0 \qquad \& \qquad \tau+\eta_x(p-\sigma)=0, \tag{114}$$

at $z=\eta(x,t)=Z\pm\frac{1}{2}h$.

We now formulate integral expressions of force and torque balance by integrating over z the equations in (113) and then the first of these expressions multiplied by $z-Z(x,t)$. Given (114) we then arrive at[5]

$$\Sigma_x=h\mathrm{G_x}, \qquad Q_x=h\mathrm{G_z}, \qquad \& \qquad M_x+\Sigma Z_x-Q=0, \tag{115}$$

where the "stress resultants" and effective moment are

$$[\Sigma,Q,M]=\int_{Z-\frac{1}{2}h}^{Z+\frac{1}{2}h}[\sigma-p,\tau,(z-Z)(\sigma-p)]\,\mathrm{d}z=\int_{Z-\frac{1}{2}h}^{Z+\frac{1}{2}h}[2\sigma,\tau,2(z-Z)\sigma]\,\mathrm{d}z+O(\epsilon^2). \tag{116}$$

The specific ordering of the stress components in (112) demands a particular form for the velocity field in order to achieve the same ordering of the strain rates (with (u,w) scaled by $\mathcal{U}$):

$$u=\epsilon[U-(z-Z)W_x]+O(\epsilon^2), \qquad w=W+O(\epsilon^2), \tag{117}$$

where $[U(x,t),W(x,t)]$ is the leading-order velocity of the centreline. Thence (with units of $\mathcal{U}/\mathcal{L}$ for strain rate), $\dot\gamma_{\mathrm{xz}}=O(\epsilon)$ and

$$\dot\gamma_{\mathrm{xx}}=2\Delta-2(z-Z)W_{xx}, \qquad \text{where} \qquad \Delta=U_x+Z_xW_x. \tag{118}$$

Given that $\dot\gamma\sim|\dot\gamma_{\mathrm{xx}}|$, for the fluid to be rigid over a section of the film at a given position in x (*i.e.* for a finite range of z), we must have that $\Delta=W_{zz}=0$. But if both these conditions hold, then $u_x=0$ across this entire cross-section. In other words, the fluid is either fully yielded or rigid across its thickness. Where yielded, we may now integrate

$$2\sigma=2\dot\gamma_{\mathrm{xx}}+B\,\mathrm{sgn}(\dot\gamma_{\mathrm{xx}}) \tag{119}$$

and $2(z-Z)\sigma$ in z to determine constitutive relations for Σ and M (the resultant Q is related to higher order corrections to the velocity field and is determined regardless by the second force balance in (115)). Before quoting the result, we note an additional

[5]Note that there are typographical errors in the corresponding formulae for order-one curvature presented by [6]. Specifically, the moment terms in (95) and (116) should be $-\epsilon\kappa M_s$, and that in (98) should be $-\kappa M_s$.

simplification implied by the velocity field in (117): the kinematic conditions at the two surfaces, $z = Z \pm \frac{1}{2}h$, reduce to $W = (Z \pm \frac{1}{2}h)_t$. Hence

$$W \equiv Z_t \qquad \& \qquad h = 1 \tag{120}$$

(in view of our scaling of the thickness). The constitutive relations are then

$$\Sigma = 4\Delta + 2B\Xi \,\mathrm{sgn}(\Delta), \qquad \Xi = \mathrm{Min}\left(1, \left|\frac{2\Delta}{W_{xx}}\right|\right), \tag{121}$$

and

$$M = -\tfrac{1}{3}W_{xx} - \tfrac{1}{2}B(1-\Xi^2)\,\mathrm{sgn}(W_{xx}). \tag{122}$$

If the fluid is rigid, on the other hand, we must have that

$$|\Sigma| < 2B\Xi \qquad \& \qquad |M| < \tfrac{1}{2}B(1-\Xi^2), \tag{123}$$

or

$$|M| < \tfrac{1}{2}B\ \mathrm{Max}\left(0, 1 - \frac{\Sigma^2}{4B^2}\right), \tag{124}$$

Equations (115) and (120)-(122) provide a theory for viscoplastic beams or columns suffering relatively small deflections (analogous to the classical Euler beam theory of elasticity [29]). With more effort, this theory can be generalized to accommodate $O(1)$ deflections (curvature) using the arc-length based coordinate system for the centreline of the beam (*cf.* §2.1 and figure 22; [6]).

4.6 Bending viscoplastic beams; toppling viscoplastic columns

Assuming that the end of the column at $x = 0$ is free (so that $\Sigma(0,t) = Q(0,t) = 0$) but that at $x = 1$ is clamped ($U(1,t) = W(1,t) = W_x(1,t) = 0$), we may write

$$(\Sigma, Q) = x(\mathrm{G_x}, \mathrm{G_z}) \qquad \& \qquad M_x = \tfrac{1}{2}\mathrm{G_z}x^2 - \Sigma Z. \tag{125}$$

If the column is initially straight, then $Z(x,0) = 0$ and

$$M(x,0) = \tfrac{1}{2}\mathrm{G_z}x^2. \tag{126}$$

The yield condition is therefore

$$\mathrm{G_z}x^2 \geq B\ \mathrm{Max}\left(0, 1 - \frac{{\mathrm{G_x}}^2x^2}{4B^2}\right). \tag{127}$$

Hence, the fixed end $x = 1$ is the most dangerous position for failure (yielding). The criterion (127) combines two effects: the viscoplastic beam can fail by bending under an imposed torque $M \to \frac{1}{2}\mathrm{G_z}$, or under the action of a compressive load $\Sigma \to \mathrm{G_x}$. The two evidently conspire, with the compressive load lowering the threshold for bending on the right of (127).

The horizontal beam, with $\mathrm{G_x} = 0$ and therefore $\Sigma(x,t) = 0$, fails purely by bending under the gravitational torque if $\mathrm{G_z} < B$. This is the viscoplastic version of Galileo's

problem for the bending of a cantilever [6]. When failure occurs, the beam bends near its fixed end over the section $\sqrt{B/\mathrm{G_z}} < x < 1$, rotating the free end down to reduce the gravitational torque. In the small deflection theory, $Z(x,t)$ increases linearly with time because $M(x,t) = \frac{1}{2}x^2$, which prescribes a time-independent vertical speed $W(x)$ through (122) (with $\Delta = \Xi = 0$). Despite this, the reduction of the gravitational torque as the beam bends down eventually allows the yield stress to terminate the beam's fall; this is illustrated in figure 23, which shows a solution of the corresponding theory for $O(1)$ deflections [6].

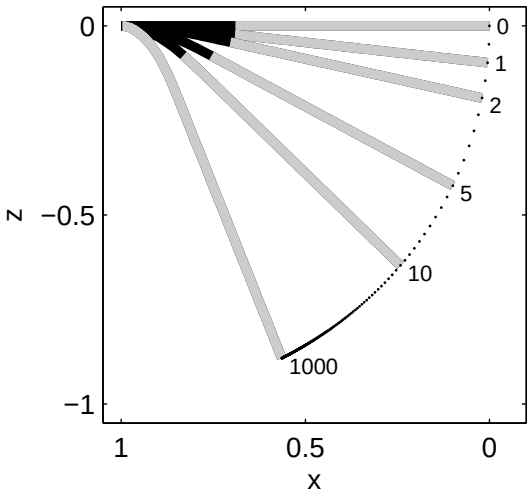

Figure 23: Sagging viscoplastic beam with $B = 0.5$ and $\mathrm{G_z} = 1$ at the times indicated. The dots show the position of the end of the beam at equally spaced times. The darker region is yielded; grey shading indicates the plug. The solution at $t = 1000$ is close to the final resting state. Note that the $x-$axis is drawn right to left in this plot, the convention in [6] (from which the solution is taken) being opposite to that used here.

The vertical column with $\mathrm{G_z} = 0$ cannot fail by bending as there is no imposed torque at $t = 0$. Instead, it collapses when $\mathrm{G_x} > 2B$, which is the criterion for a slender vertical filament to yield symmetrically at its base [5]. Once the column fails in that fashion, any deviation of its orientation from the vertical will allow it to topple over sideways. The situation is rather different to the Euler buckling problem of elasticity theory, which is classically posed as a linear instability problem. For the viscoplastic problem, as one moves beyond the threshold for failure $\mathrm{G_x} = 2B$, a narrow region yields at the base of the column. This region expands linearly with time as deflections grow explosively, corresponding to sudden toppling of the column; see the illustrative solution for $O(1)$ curvature in figure 24 and [6] for further details. An interesting possible application of this problem is in 3D printing [22].

5 Concluding remarks

These notes have presented an array of asymptotic analyses of viscoplastic flow problems, together with a sprinkling of other mathematical techniques. In almost all the problems in question, and as illustrated in several instances, the more analytical methodologies work hand-in-hand with numerical approaches (discussed by A. Wachs) to acquire a detailed understanding of the viscoplastic flow dynamics. We enjoyed slot flows, boundary layers, sticky and slippy films, and bending columns, highlighting the important effects introduced by the yield stress in each case. The emphasis has been on asymptotics and therefore on building approximate solutions, and complements approaches seeking to constrain solutions

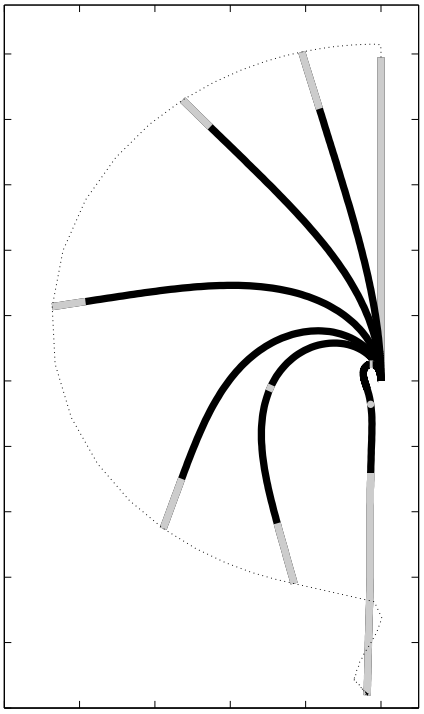

Figure 24: A viscoplastic column buckling under gravity with $B = \mathrm{G_x} = 1$ at the times $t = 0$, 0.41, 0.4125, 0.415, 0.4175, 0.42 and 1. To initiate collapse, the column is extruded almost upwards at fixed speed such that it reaches the critical length for collapse at $t = 0$; the direction of extrusion is offset from the vertical by an angle 10^{-6} to allow sideways toppling. The dotted curve shows the position of the free end of the column. The darker region is yielded; grey shading indicates the plug. At later times, the column is hanging vertically and begins to stretch and thin under gravity (*i.e.* $h(x,t) \neq 1$; another ingredient of the generalized theory)

with variational and bounding techniques, as reviewed by I. Frigaard.

Acknowledgements: I thank two Hewitts for their contributions to the work summarized in these notes: Ian Hewitt computed and prepared figures 5, 20 and 21. Duncan Hewitt computed and prepared figures 8, 11–14. Section 3 is a prelude to a more thorough discussion by a Focussed Research Group on Viscoplastic Fluids, which was established at Banff, October 2015. I thank Richard Craster for the construction of the slipline field in figure 12. Lujia Liu contributed to the developments of §4.4.

References

[1] M. G. Alishaev, V. M. Entov, and A. E. Segalov, *Elementary solutions of plane nonlinear filtration problems*, Fluid Dynamics, 4 (1969), pp. 77–84.

[2] N. J. Balmforth and R. V. Craster, *A consistent thin-layer theory for Bingham plastics*, J. Non-Newtonian Fluid Mechanics, 84 (1999), pp. 65–81.

[3] N. J. Balmforth, R. V. Craster, P. Perona, A. C. Rust, and R. Sassi, *Viscoplastic dam breaks and the Bostwick consistometer*, J. Non-Newtonian Fluid Mechanics, 142 (2007), pp. 63–78.

[4] N. J. Balmforth, R. V. Craster, A. C. Rust, and R. Sassi, *Viscoplastic flow over an inclined surface*, J.Non-Newtonian Fluid Mech., 142 (2007), pp. 219–243.

[5] N. J. Balmforth, N. Dubash, and A. C. Slim, *Extensional dynamics of viscoplastic filaments: I and II*, J. Non-Newtonian Fluid Mech., 165 (2010), pp. 1139–1146 and 1147–1160.

[6] N. J. Balmforth and I. J. Hewitt, *Viscoplastic sheets and threads*, Journal of Non-Newtonian Fluid Mechanics, 193 (2013), pp. 28–42.

[7] N. J. Balmforth and R. R. Kerswell, *Granular collapse in two dimensions*, Journal of Fluid Mechanics, 538 (2005), pp. 399–428.

[8] H. A. Barnes, *A review of the slip (wall depletion) of polymer solutions, emulsions and particle suspensions in viscometers: its cause, character, and cure*, Journal of Non-Newtonian Fluid Mechanics, 56 (1995), pp. 221–251.

[9] C. M. Bender and S. A. Orszag, *Advanced Mathematical Methods for Scientists and Engineers*, McGraw-Hill, 1978.

[10] M. G. Bernadiner and A. L. Protopapas, *Progress on the theory of flow in geologic media with threshold gradient*, J. of Environmental Science & Health Part A, 29 (1994), pp. 249–275.

[11] S. H. Bittleston, J. Ferguson, and I. A. Frigaard, *Mud removal and cement placement during primary cementing of an oil well: Laminar non-Newtonian displacements in an eccentric annular Hele-Shaw cell*, J. Engineering Mathematics, 43 (2002), pp. 229–253.

[12] J. Bleyer and P. Coussot, *Breakage of non-Newtonian character in flow through a porous medium: Evidence from numerical simulation*, Phys. Rev. E, 89 (2014), p. 063018.

[13] J. Boujlel, M. Maillard, A. Lindner, G. Ovarlez, X. Chateau, and P. Coussot, *Boundary layer in pastes: displacement of a long object through a yield stress fluid*, Journal of Rheology, 56 (2012), pp. 1083–1108.

[14] J. A. Chamberlain, J. E. Sader, K. A. Landman, and L. R. White, *Incipient plane-strain failure of a rectangular block under gravity*, Int. J. of Mechanical Sciences, 43 (2001), pp. 793–815.

[15] T. Chevalier, C. Chevalier, X. Clain, J. C. Dupla, J. Canou, S. Rodts, and P. P. Coussot, *Darcy's law for yield stress fluid flowing through a porous medium*, J. Non-Newtonian Fluid Mech., 195 (2013), pp. 57–66.

[16] T. Chevalier, S. Rodts, X. Chateau, J. Boujlel, M. Maillard, and P. Coussot, *Boundary layer (shear-band) in frustrated viscoplastic flows*, Europhysics Letters, 102 (2013), p. 48002.

[17] G. H. Covey and B. R. Stanmore, *Use of the parallel-plate plastometer for the characterisation of viscous fluids with a yield stress*, Journal of Non-Newtonian Fluid Mechanics, 8 (1981), pp. 249–260.

[18] R. V. Craster and O. K. Matar, *Dynamics and stability of thin liquid films*, Reviews of modern physics, 81 (2009), p. 1131.

[19] V. M. Entov, *Analogy between equations of plane filtration and equations of longitudinal shear of nonlinearly elastic and plastic solids*, Journal of Applied Mathematics and Mechanics, 34 (1970), pp. 153–164.

[20] E. D. Fernández-Nieto, P. Noble, and J.-P. Vila, *Shallow water equations for non-newtonian fluids*, Journal of Non-Newtonian Fluid Mechanics, 165 (2010), pp. 712–732.

[21] L. Fusi, A. Farina, and F. Rosso, *Flow of a Bingham-like fluid in a finite channel of varying width: a two-scale approach*, Journal of Non-Newtonian Fluid Mechanics, 177 (2012), pp. 76–88.

[22] C. J. Hansen, W. Wu, K. S. Toohey, N. R. Sottos, S. R. White, and J. A. Lewis, *Self-healing materials with interpenetrating microvascular networks*, Advanced Materials, 21 (2009), pp. 4143–4147.

[23] D. R. Hewitt, M. Daneshi, N. J. Balmforth, and D. M. Martinez, *Obstructed and channelized viscoplastic flow in a hele-shaw cell*, J. Fluid Mechanics, 790 (2016), pp. 173–204.

[24] I. J. Hewitt and N. J. Balmforth, *Viscoplastic lubrication theory with application to bearings and the washboard instability of a planing plate*, J. Non-Newtonian Fluid Mech., 169 (2012), pp. 74–90.

[25] E. J. Hinch, *Perturbation Methods*, Cambridge University Press, 1991.

[26] M. Jalaal, N. J. Balmforth, and B. Stoeber, *Slip of spreading viscoplastic droplets*, Langmuir, 31 (2015), pp. 12071–12075.

[27] G. G. Lipscomb and M. M. Denn, *Flow of Bingham fluids in complex geometries*, Journal of Non-Newtonian Fluid Mechanics, 14 (1984), pp. 337–346.

[28] K. F. Liu and C. C. Mei, *Slow spreading of a sheet of Bingham fluid on an inclined plane*, J . Fluid Mech., 207 (1989), pp. 505–529.

[29] E. H. Mansfield, *The bending and stretching of plates*, Cambridge University Press, 2005.

[30] J. F. Nye, *The mechanics of glacier flow*, J. Glaciol, 2 (1952), pp. 82–93.

[31] ——, *Plasticity solution for a glacier snout*, J. Glaciol, 6 (1967), pp. 695–715.

[32] J. G. Oldroyd, *Two-dimensional plastic flow of a Bingham solid*, Mathematical Proceedings of the Cambridge Philosophical Society, 43 (1947), pp. 383–395.

[33] S. Pelipenko and I. A. Frigaard, *Two-dimensional computational simulation of eccentric annular cementing displacements*, IMA journal of applied mathematics, 69 (2004), pp. 557–583.

[34] J.-M. Piau, *Viscoplastic boundary layer*, Journal of non-Newtonian fluid mechanics, 102 (2002), pp. 193–218.

[35] O. Pinkus and B. Sternlicht, *Theory of hydrodynamic lubrication*, McGraw-Hill, 1961.

[36] W. Prager and P. G. Hodge, *Theory of Perfectly Plastic Solids*, Dover, 1968.

[37] A. Putz, I. A. Frigaard, and D. M. Martinez, *The lubrication paradox & use of regularisation methods for lubrication flows*, Journal of Non-Newtonian Fluid Mechanics, 163 (2009), pp. 62–77.

[38] M. F. Randolph and G. T. Houlsby, *The limiting pressure on a circular pile loaded laterally in cohesive soil*, Géotechnique, 34 (1984), pp. 613–623.

[39] A. Roustaei, A. Gosselin, and I. A. Frigaard, *Residual drilling mud during conditioning of uneven boreholes in primary cementing. part 1: Rheology and geometry effects in non-inertial flows*, Journal of Non-Newtonian Fluid Mechanics, 220 (2015), pp. 87–98.

[40] C. Schoof and I. A. Hewitt, *Ice-sheet dynamics*, Annual Review of Fluid Mechanics, 45 (2013), pp. 217–239.

[41] D. N. Smyrnaios and J. A. Tsamopoulos, *Squeeze flow of Bingham plastics*, Journal of Non-Newtonian Fluid Mechanics, 100 (2001), pp. 165–190.

[42] ——, *Transient squeeze flow of viscoplastic materials*, Journal of Non-Newtonian Fluid Mechanics, 133 (2006), pp. 35–56.

[43] I. N. Sneddon, *Elements of Partial Differential Equations*, McGraw-Hill, 1957.

[44] L. Talon and D. Bauer, *On the determination of a generalized Darcy equation for yield-stress fluid in porous media using a Lattice-Boltzmann TRT scheme.*, The European Physical Journal E, 36 (2013), p. 139.

[45] D. L. Tokpavi, A. Magnin, and P. Jay, *Very slow flow of Bingham viscoplastic fluid around a circular cylinder*, Journal of Non-Newtonian Fluid Mechanics, 154 (2008), pp. 65–76.

[46] I. C. Walton and S. H. Bittleston, *The axial flow of a Bingham plastic in a narrow eccentric annulus*, Journal of Fluid Mechanics, 222 (1991), pp. 39–60.

[47] G. B. Whitham, *Linear and nonlinear waves*, Wiley, 1974.

[48] S. Wilson, *A note on thin-layer theory for Bingham plastics*, Journal of Non-Newtonian Fluid Mechanics, 1 (1999), pp. 29–33.